

Local comparisons of tropospheric ozone: Vertical soundings at two neighbouring stations in Southern Bavaria

Thomas Trickl¹, Martin Adelwart², Dina Khordakova³, Ludwig Ries⁴, Christian Rolf³,
Michael Sprenger⁵, Wolfgang Steinbrecht² and Hannes Vogelmann¹

¹Karlsruher Institut für Technologie, Institut für Meteorologie und Klimaforschung (IMK-IFU), Kreuzeckbahnstr. 19, D-82467 Garmisch-Partenkirchen, Germany

²Deutscher Wetterdienst, Meteorologisches Observatorium, Albin-Schwaiger-Weg 10, 82383 Hohenpeißenberg, Germany

³Forschungszentrum Jülich, IEK-7, Wilhelm-Johnen-Straße, 52425 Jülich, Germany

⁴Umweltbundesamt II 4.5, Plattform Zugspitze, GAW-Globalobservatorium Zugspitze-Hohenpeißenberg, Schneefernerhaus, 82475 Zugspitze, Germany

⁵Eidgenössische Technische Hochschule (ETH) Zürich, Institut für Atmosphäre und Klima, Universitätstraße 16, 8092 Zürich, Switzerland

Correspondence to: Dr. Thomas Trickl, thomas@trickl.de, Thomas-Knorr-Str. 47, D-82467 Garmisch-Partenkirchen, Germany; tel. +49-8821-50283; Dr. Hannes Vogelmann, hannes.vogelmann@kit.edu, Karlsruher Institut für Technologie, IMK-IFU, Kreuzeckbahnstr. 19, D-82467 Garmisch-Partenkirchen, Germany; tel. +49-8821-258

Abstract. In this study ozone profiles of the differential-absorption lidar at Garmisch-Partenkirchen are compared with those of ozone sondes of the Forschungszentrum Jülich and of the Meteorological Observatory Hohenpeißenberg (German Weather Service). The lidar measurements are quality assured by the highly accurate nearby in-situ ozone measurements at the Wank (1780 m a.s.l.) and Zugspitze (2962 m a.s.l.) summits and at the Global Atmosphere Watch station Schneefernerhaus (UFS, 2670 m a.s.l.), at distances of 9 km or less from the lidar. The mixing ratios of the lidar results agree almost perfectly with those of the monitoring stations within ± 3 ppb, with a slight positive offset of $0.6 \text{ ppb} \pm 0.6 \text{ ppb}$ (varying with year and station) conforming to the known -1.8% calibration bias of the in-situ instruments. Side-by-side soundings of the lidar and electrochemical (ECC) sonde measurements in February 2019 by a team of the Forschungszentrum Jülich shows just small positive ozone offsets for the sonde ($\leq 3.4 \text{ ppb}$) and an agreement to within just $\pm 2.5 \text{ ppb}$ in the troposphere after applying an altitude-independent bias correction, which we regard as the wintertime uncertainty of the lidar, almost constant within the troposphere. We conclude that the recently published uncertainties of the lidar in the final configuration since 2012 are realistic and rather small for low to moderate ozone. Comparisons of the lidar with the Hohenpeißenberg routine Brewer-Mast sonde measurements with Brewer-Mast sondes are more demanding because of the distance of 38 km between both sites implying significant ozone differences in some layers, particularly in summer. These Our comparisons cover the three years September 2000 to August 2001, 2009 and 2018. A slight negative average offset ($-3.64 \text{ ppb} \pm 7.5 \text{ ppb}$ (~~full error~~maximum of deviations)) of the sondes with respect to the lidar is found. Most sonde ~~measurements data~~ could be improved in the troposphere by recalibration with the Zugspitze station data (until 2011 summit, afterwards UFS). This would not only remove the average offset, but also greatly reduce the variability of the individual offsets. The comparison for 2009 suggests a careful partial re-evaluation of the lidar measurements between 2007 and 2011 for altitudes above 6 km where ~~an~~ occasionally a negative bias occurred.

Key words: Tropospheric ozone, ozone sonde, ozone lidar, differential absorption

Trupdwluw#kuliw@wkwxuvly

41 **1. Introduction**

42 The development of tropospheric ozone has been studied over more than a century (e.g., Gaudel et al., 2018;
43 Tarasick et al., 2019). For many decades, balloon-borne ozone sondes have been a primary work horse of ozone
44 profiling. Their measurement principle is based on the oxidation of iodide (I⁻) to iodine (I₂) by ozone in a wet-
45 chemical potassium iodide (KI) cell. Between cathode and anode of the wet-chemical cell, the oxidation reaction
46 drives an electrical current which can be measured (two electrons per ozone molecule). Recently, nearly all
47 stations have used the so-called ECC (electro-chemical-cell) sonde type (Komhyr 1969; 1995), featuring two
48 cells with different potassium iodide concentrations (anode and cathode cell). Only the Hohenpeißenberg station,
49 discussed here, still uses the older-type Brewer-Mast sondes (Brewer and Milford, 1960), which uses one cell
50 only (with a platinum cathode and a silver anode), and a less efficient pump design (Steinbrecht et al., 1998).
51 Ozone sondes have been characterized in numerous studies, both in flight (e.g., Attmannspacher and Dütsch,
52 1981; De Muer and Malcorps, 1984; Beekmann et al., 1994; Kerr et al., 1994; Jeannot et al., 2007; in recent
53 years: Gaudel et al., 2015; Van Malderen et al., 2016; Deshler et al., 2017; Tarasick et al., 2021; Ancellet et al.,
54 2022; Stauffer et al., 2022), and in a laboratory simulation chamber (Smit et al., 2007, 2014, 2021). Generally,
55 the relative uncertainty of individual ECC soundings for ozone in the mid-latitude troposphere is about 5 to 10%
56 (Logan et al., 2012; Smit et al., 2014; Tarasick et al., 2016, 2019). Following rigorous best practices, 5%
57 accuracy can be achieved (Vömel et al., 2020; Smit et al., 2021; Tarasick et al., 2019; 2021). For Brewer-Mast
58 soundings, the relative uncertainty in the troposphere is slightly higher, about 10 to 15% (Smit et al. 2014;
59 Tarasick et al., 2016, 2019).

60 The ozone soundings at the Meteorological Observatory Hohenpeißenberg (MOHp) of the German Weather
61 Service (Deutscher Wetterdienst, DWD) in Southern Bavaria have been routinely carried out since November
62 1966, yielding one of the longest ozone-sonde time series. Brewer-Mast ozone sonde data tend to have a low
63 bias above about 25 km altitude (Steinbrecht et al., 1998). In the troposphere, compared to ECC soundings,
64 Tarasick et al. (2002, 2016) ~~find~~ found a negative bias of about 20 % for ozone from Canadian Brewer-Mast
65 soundings prior to 1980. European Brewer-Mast stations, however, have generally used a much more extensive
66 preparation procedure for their sondes (Claude et al. 1987), and no significant tropospheric bias has been
67 reported for their routine Brewer-Mast soundings (de Backer et al. 1998; Stübi et al. 2008; Logan et al., 2012), as
68 well as in chamber experiments (Smit et al., 2014).

69 Routine measurements with ozone sondes yield time series free of a fair-weather sampling bias. However, the
70 balloon ascents take place at intervals of several days. Ozone profiles at short intervals (less than one minute to
71 several minutes) can be provided by lidar sounding, but are limited to clear atmospheric conditions. Lidar
72 measurements can generate altitude-time curtain plots and, thus, give much better insight into the impact of
73 atmospheric transport (e.g., Browell et al., 1987; Ancellet et al., 1991; Langford et al., 1996).

74 At IFU (Fraunhofer-Institut für Atmosphärische Umweltforschung; now: Karlsruher Institut für Technologie,
75 IMK-IFU) in Garmisch-Partenkirchen (Germany), a differential-absorption lidar (DIAL) with a particularly wide
76 operating range from next to the ground up to the upper troposphere was completed in 1990 in the framework of
77 the TESLAS (Tropospheric Environmental Studies by Laser Sounding) subproject of EUROTRAC (TESLAS,
78 1997; EUROTRAC, 1997, Kempfer et al., 1994). Subsequently, the system was applied for a full year (1991)
79 within the TOR (Tropospheric Ozone Research; Kley et al., 1997) subproject of EUROTRAC (Carnuth et al.,
80 2002). The operating range of this system was extended upwards to roughly 15 km in 1994 by introducing three-
81 wavelength operation (Eisele et al., 1999). Due to its design, the IFU ozone DIAL features particularly low
82 uncertainties.

83 Until 2003 the system was used for individual research projects. Between 2007 and 2018 routine measurements
84 took place, parallel to lidar measurements of water vapour (Vogelmann and Trickl, 2008) and aerosol (Trickl et
85 al., 2020b). The complementary information from these instruments has made possible a large number of
86 investigations related to atmospheric transport. The IFU ozone DIAL was recently fully described by Trickl et al.
87 (2020a).

88 The distance between MOHp and IFU is just 38 km which offers a good chance for comparisons. ~~Due to its~~
89 ~~design, the IFU ozone DIAL features particularly low uncertainties.~~ However, such a comparison must be made
90 with care since the atmospheric variability is high on a rather small temporal and spatial scale (Vogelmann et al.,
91 2011; 2015), mostly caused by the advection of air masses from rather different source region and altitudes, with
92 different concentrations (e.g., Stohl and Trickl, 1999; Trickl et al., 2003; Trickl et al., 2011). The variability of
93 the vertical distribution of ozone measurements rarely yields very strong concentration changes, but the
94 concentration changes are extreme for water vapour. Our lidar measurements of water vapour exhibit a
95 concentration span of more than two decades, with minima of the relative humidity (RH) clearly below 1 % in
96 layers descending from the stratosphere (Trickl et al., 2014; 2015; 2016; Klanner et al., 2021).

97 Comparisons between the MOHp sonde and the IFU ozone lidar were made in the second half of the 1990s and
98 in 2001, after the first upgrading of the lidar A few of these comparisons in 1996 and 1997 were published by
99 Eisele et al. (1997; 1999). For the six cases with supposedly sufficient air-mass matching a principal agreement
100 in the middle and upper troposphere to within 5 ppb prevailed with occasional departures of the order of 10 ppb.

101 ~~Afterwards just routine comparisons with the nearby summit stations were made. Until 2010 the lidar results~~
102 ~~were compared with the long-term measurements at Wank and Zugspitze. Apart from occasional orographically~~
103 ~~induced deviations an agreement mostly to within ± 2 ppb was found. After these in-situ measurements were~~
104 ~~terminated the lidar measurements were compared with the ozone measurements at UFS. Mostly a similar~~
105 ~~agreement was found.~~

106 ~~However, the need for a validation of the lidar also at higher altitudes has been obvious. Such an effort became~~
107 ~~more and more attractive with the growing technical performance of the system. In addition, hints on ozone~~
108 ~~differences between the Zugspitze (2962 m a.s.l.) in-situ data and the MOHp values (H. E. Scheel, personal~~
109 ~~communication around 2010) for 3 km a.s.l. have led to a revived interest in a thorough comparison. There have~~
110 ~~been speculations about an influence of a different air composition outside the mountains at low altitudes up to a~~
111 ~~few kilometres.~~

112 In this paper we first characterize the lidar performance by side-by-side ascents of ozone-sondes by a team of the
113 Forschungszentrum Jülich (FZJ). Then, we give a statistical assessment for the measurements at IFU and MOHp
114 for 2018. For this year we achieved the best coverage ~~of~~ by DIAL measurements. This allows us to make an air-
115 mass related data selection to improve the comparison. After the shutdown of the IFU summit stations in 2012,
116 comparisons have been made exclusively with the Global Atmosphere Watch (GAW) routine in-situ
117 measurements at the Schneefernerhaus high-altitude station (Umweltforschungsstation Schneefernerhaus, UFS,
118 2671 m a.s.l.). UFS is located just below the Zugspitze summit. Finally, we also compare lidar and MOHp sonde
119 for two earlier development phases of the lidar, for which ozone reference data at the local summit stations
120 Wank (1780 m a.s.l.) and Zugspitze exist.

121 2. Methods

122 2.1 Brewer-Mast sonde system at Hohenpeißenberg

Trupdwlhu#f#kuliw@l#k#xuvly

Trupdwlhu#f#kuliw@l#k#xuvly

Trupdwlhu#f#kuliw@l#k#xuvly

123 MOHp (975 m a.s.l., 47.80 N, 11.00 E) is located on an isolated mountain outside the Alps, 38 km to the north of
124 IMK-IFU and 50 km to the south-west of Munich (~~975 m a.s.l., 47.80 N, 11.00 E~~). Brewer-Mast ozone sondes
125 have been launched on a regular basis since November 1966. The sondes undergo a rigorous preparation
126 procedure (Claude et al. 1987), which has remained essentially unchanged since the early 1970s. From 1995 to
127 2005, Vaisala RS80 radiosondes and a Vaisala PC-CORA ground station have been used in combination with
128 the ozone sondes. This was changed to Vaisala RS92 radiosondes and DigiCora III MW31 ground equipment in
129 2005, to MW41 ground station in 2018, and to Vaisala RS41 radiosondes in 2019. The standard processing does
130 not subtract a background current, but ozone sondes with non-negligible background current on the ground
131 (corresponding to 2.5 ppb ozone and more) are not flown. The background of most sondes launched is well
132 below this threshold. Pump temperature is assumed to be constant at 300 K, which compensates to some degree
133 for a too weak pump correction in the stratosphere (Steinbrecht et al. 1998). The time lag is comparable to that of
134 ECC sondes (about 20 s; see Vömel et al., 2020). A time-lag correction is not applied, but this is not critical
135 outside regions with steep ozone gradients since the corresponding vertical shift is just of the order of 0.1 km.
136 Each ozone profile is adjusted by multiplication with an altitude-independent correction factor (typically around
137 1.08, standard deviation 5 %), so that the total ozone column estimated from the sounding (including an
138 extrapolation above approximately 30 km) matches the more accurate total ozone measurement from on-site
139 Dobson or Brewer spectrometers, or from satellite instruments. This so-called “Dobson correction” generally
140 improves that accuracy of the ozone sounding data in the stratosphere, but may introduce a small bias in the
141 tropospheric data of some soundings (e.g., Stübi et al., 2008; Logan et al. 2012).
142 The MOHp ozone-sonde and radiosonde data are stored in the data base of the Network for the Detection of
143 Atmospheric composition change (NDACC), from where they were imported for the study presented here.

144 2.2 ECC sonde system of the Forschungszentrum Jülich (FZJ)

145 A mobile balloon-borne sonde system of FZJ was operated at IMK-IFU (at 730 m a.s.l.), in close vicinity to the
146 ozone DIAL (35 m), during the FIRMOS (Far Infrared Radiation Mobile Observation System) measurement
147 campaign (Klanner et al., 2020; Palchetti et al., 2021; Di Natale, 2021; Belotti et al., 2023). Several balloons
148 with cryogenic frostpoint hygrometers (CFH; Vömel et al., 2007; 2016), standard Vaisala RS-41-SGP
149 radiosondes (Vaisala et al., 2019), En-Sci ECC ozone sondes (Komhyr et al., 1995; Smit et al., 2007) and
150 COBALD backscatter sondes (Brabec, 2011) were launched. The data were transmitted to a ground station
151 installed for this campaign at the Zugspitze summit. The combined balloon payload is well tested and regularly
152 also used by the GCOS Reference Upper Air Network (GRUAN) (e.g., Dirksen et al., 2014).

153 We followed the standard operating procedures (SOP) of Smit et al. (2014) for the sonde preparation using a
154 solution composition of 1 % and 1/10 (one-tenth) buffer for best results with sondes from the manufacturer En-
155 Sci (Thompson et al., 2019).

156 For the analysis of the ECC data, the methods described by Vömel et al. (2020) are used, i.e., time lag correction
157 and background current correction. The overall uncertainty of the ozone measurements of the ECC sondes is 5%.
158 Due to the obstruction of the line of sight between launch site at IMK-IFU and the ground station at the
159 summit by the Waxenstein mountain allowed data recording only from approximately 1500 m altitude upwards.
160 Therefore, we used the estimated ECC background current from the sonde preparation one day before a flight as
161 starting value for the background correction instead of the actual measured profile from ground up to 1500 m.
162 This results in an additional uncertainty in the lower part of the profile (2 to 3 km a.s.l.).

163 2.4 IFU ozone DIAL system

164 The ozone DIAL of IMK-IFU (Garmisch-Partenkirchen), located at 47.477 N, 11.064 E, and 740 m a.s.l., has
165 been developed and optimized since 1988 (Kempfer et al., 1994; Trickl et al., 2020a). It is based on a krypton
166 fluoride excimer laser, operated at 400 mJ per pulse (40 W) of narrowband radiation at 248.5 nm, two
167 Newtonian receiving telescopes (diameter of the primary mirrors: 0.13 m and 0.5 m) and 1.1-m grating
168 spectrographs for wavelength separation. Efficient stimulated Raman shifting in hydrogen and deuterium yields
169 emission at the three operating wavelengths 277.2 nm, 291.8 nm and 313.2 nm. The shorter-wave spectral
170 components are absorbed by ozone (“on” wavelengths), that at 313.2 nm (“off” or reference wavelength) is
171 almost outside the absorption region of O₃. The laser system is operated with a repetition rate of 99 Hz which
172 allows a short data-acquisition time of just 41 s for the maximum number of 4096 laser shots accepted by the 24-
173 bit memory of the electronics. More shots are advisable under noisy daytime conditions in summer, but a longer
174 acquisition was prevented by laser issues.

175 The data evaluation is based on differentiating the backscatter signals, which is highly sensitive to the noise and
176 imperfections of the raw data (stored in 7.5-m bins). Therefore, the generated ozone profiles are smoothed with a
177 numerical filter. The noise fraction in the strongly decreasing backscatter signal grows with altitude. Thus, the
178 smoothing interval must be dynamically enhanced towards the tropopause (yielding a vertical resolution 0.05 to
179 0.5 km). The entire procedure is described in detail by Trickl et al. (2020a).

180 The shortwave 277.2-nm emission yields particularly accurate measurements, but the strong extinction of this
181 radiation by ozone limits the range to about 8 km. The performance in the two 277.2-nm channels is robust with
182 respect to minor misalignment, with uncertainties of about 2 to 3-4 ppb up to 5 km (the estimated uncertainties
183 are listed in Table 4 of Trickl et al. (2020a)). This is not the case for 291.8 nm where the optical alignment must
184 be controlled with care because of less tight focussing into the entrance slit of the far-field spectrograph. In
185 addition, the 291.2-nm backscatter signal is three times noisier than that for 277.2-nm which necessitates
186 stronger smoothing of the retrieved ozone profiles (Trickl et al., 2020a). For 5 to 8 km we specify uncertainties
187 of 3 to 7 ppb. The noise of the 313.2-nm signal becomes important at large distances. As a consequence, the
188 uncertainty of the ozone mixing ratio can become rather high in the upper troposphere and the tropopause
189 region, in particular in summer due to the stronger loss of signal caused by the higher levels of ozone.
190 Sometimes the uncertainty just below the tropopause can even exceed 10 ppb.

191 The DIAL data processing is made for different wavelength combinations (Eisele and Trickl, 2005). ~~In this~~
192 ~~way~~By comparing the resulting ozone profiles, an internal quality control can be achieved. The optical alignment
193 is optimized immediately after detecting an ozone mismatch in the first quicklook data evaluation. Just the laser
194 beam overlap of the different wavelength components (Trickl et al., 2020a) and the beam pointing must be
195 optimized.

196 The calibration of the ozone lidar measurements has been based from the very beginning (1991) on the accurate
197 temperature-dependent ozone absorption cross sections of the University of Reims (Daumont et al., 1992;
198 Malicet et al., 1995). These cross sections were verified for four wavelengths below 300 nm by Viallon et al.
199 (2015) to within ±0.06 %. In the presence of aerosol an aerosol correction is made with the algorithms of Eisele
200 and Trickl (2005). This correction is rather robust for the wavelength pair 277 nm - 292 nm because of the strong
201 absorption at the short “on” wavelength and the moderate wavelength difference (Völger et al., 1996).
202 Meteorological data for calculating density and temperature profiles are taken from the Munich radiosonde
203 (station 10868). The retrieved 313-nm aerosol backscatter coefficients have been routinely stored in the data
204 base of the European Aerosol Lidar Network (EARLINET) since 2007.

205 After repeated system upgrading the final performance of the lidar was reached in late 2012. In the absence of
206 aerosol the far-field ozone could be evaluated with high reliability from the 291.9-nm signal alone, after
207 precisely modelling the air number density from radiosonde data (Trickl et al., 2020). In this way the daytime
208 noise ~~caused by the high solar background induced by the division by~~ the 313-nm ~~data-reference profiles~~ in
209 summer could frequently be avoided.

210 During the final decade of the lidar operation a fitting procedure was applied in noisy situations in the upper
211 troposphere (i.e., under high-ozone conditions in summer). This procedure reduces unrealistic curvature of ozone
212 structures caused by enhanced data smoothing, and, thus, abrupt concentration changes (in particular at the
213 tropopause) visible in the raw data are reproduced in the mixing ratio. ~~We prepared an extension of the data-~~
214 ~~acquisition time from 41 s to about five minutes in order to improve the signal-to-noise ratio. However, the lidar~~
215 ~~operation ended before the start of this option.~~

216 From 1991 to 2003 the DIAL was operated for focussed research projects. Routine measurements took place
217 from 2007 to 2018, until 2015 parallel to measurements with a water-vapour DIAL (Trickl et al., 2014, 2015,
218 2016, 2020b). In 2012 the highest data quality was finally reached, which included significant improvements for
219 the near-field telescope (Trickl et al., 2020a). Thus, the conditions for a meaningful system validation were
220 obtained. The operation was discontinued in February 2019, after the retirement of the first author of this paper.

221 ~~2.5 In-situ High-elevation surface measurements observations~~

222 Quality-assured ozone measurements at the ~~summit stations~~ Wank (1780 m a.s.l., 7.0 km to the north-east of
223 IMK-IFU, 47.511° N, 11.141° E) and Zugspitze (2962 m a.s.l., 8.4 km to the south-west of IMK-IFU, 47.421° N,
224 10.986° E) took place from 1978 to 2012. Since the 1990s, two or three TE 49 ~~ozone~~ analysers (Thermo
225 Environmental Instruments, USA) were operated simultaneously at each station. These instruments are based on
226 ultraviolet (UV) absorption at 253.65 nm. Several comparisons using transfer standards (O₃ calibrators TE 49
227 PS) were made with the World Meteorological Organization (WMO) Global Atmosphere Watch (GAW)
228 reference instrument kept at the WMO/GAW calibration centre operated by EMPA, Switzerland (Klausen et al.,
229 2003). The most recent comparison was conducted in June 2006 and confirmed that the Zugspitze O₃ data are on
230 the GAW scale.

231 Apart from the two mountain stations measurements were performed also at IFU at about 740 m a.s.l. (47.477°
232 N, 11.064° E). This laboratory was adjacent to that of the ozone DIAL.

233 At UFS (0.70 km to the south-east of Zugspitze, 47.417°, 10.980° E) ozone has been continuously measured
234 since 2002 by a team of the German ~~Federal~~-Environment Agency (Umweltbundesamt, UBA) using TEI 49i
235 instruments (Thermo Electron Corporation). The gas inlet is at 2671 m a.s.l. ~~As ozone standard for weekly and~~
236 ~~monthly calibration a TEI 49C-PS instrument was applied that was calibrated against the ozone standard of UBA~~
237 ~~(UBA SRP#29) on an annual basis. For weekly and monthly calibration of the ozone measurements a TEI 49C-~~
238 ~~PS station ozone calibrator was applied. This primary standard was annually adjusted to the German ozone~~
239 ~~standard operated by UBA (UBA 204 SRP#29). UBA operates the German standard for Ozone. It that~~ was
240 adjusted via BIPM (Bureau International des Poids et Mesures) in Paris to the NIST ozone reference standard of
241 ~~the WMO/GAW measurement programme~~GAW. The measurements were supported by a second instrument
242 (Horiba APOA-370) ~~which is equivalent to the TEI-49i. The instrumentation is fully adequate for Global~~
243 ~~Atmosphere Watch monitoring. GAW system and~~GAW performance audits at the station for surface ozone took
244 place in 2001, 2006, and 2011 and 2020 (Zellweger et al., 2001; 2006; 2011; 2020).

IrupidwluhWfEkuIiw@uEckWxuvly

IrupidwluhWfEkuIiw@uEckWxuvly

IrupidwluhWfEkuIiw@uEckWhw

IrupidwluhWfEkuIiw@uEckWxuvly

245 The uncertainty of the ~~in-situ ozone measurements is ± 0.5 ppb with respect to the WMO standard (Hearn et al.,~~
 246 ~~1961)~~. This fulfills the GAW requirement.

247 The ozone data for all sites are stored at half-hour intervals. The times are specified for the end of the averaging
 248 interval in Central European Time (CET, = UTC + 1 h). 1-h averages for the Zugspitze stations were made
 249 available to the World Data Center and the TOAR data base (Schultz et al., 2017). In the present study we use
 250 data at half-hour time resolution. ~~The ozone series at the two Zugspitze sites have been discussed on two recent~~
 251 ~~scientific studies (1970 to 2020; Parrish et al., 2019; Trickl et al., 2023).~~

252 2.6 LAGRANTO Trajectories

253 Fifteen-day backward trajectories were calculated with the Lagrangian Analysis tool (LAGRANTO; Sprenger
 254 and Wernli, 2015; Wernli and Davies 1997). The driving wind fields are obtained from the ERA5 reanalysis
 255 dataset (Hersbach et al., 2020), which we interpolated to a 0.5° latitude/longitude grid, and on 137 vertical hybrid
 256 levels. The input ERA5 data are available at a one-hour temporal resolution; the output positions of the
 257 trajectories are written at 15-min time interval to allow for a more refined analysis. The start coordinates of the
 258 backward trajectories are 11.064 E, 47.477 N, and the start altitudes match the altitudes of interest in the
 259 soundings (see Sect. 4). The start times of the trajectories correspond to the sounding times within five minutes.
 260 Finally, the start times are also shifted by several hours relative to the sounding time to assess the sensitivity of
 261 the trajectory calculation on time.

262 3. Results

263 The main problem in comparing vertical sounding ~~instruments~~ is illustrated in Fig. 1 which shows several ozone
 264 measurements at Garmisch-Partenkirchen and Hohenpeißenberg in the morning of 2 October 2017. The vertical
 265 distributions during that period are characterized by a descending stratospheric intrusion layer (see low relative
 266 humidity) of rapidly diminishing width and significant changes at all altitudes on a short time scale. This reveals
 267 ~~the a considerable spatially highly inhomogeneity of the~~ air mass. The approximate agreement of lidar and
 268 Hohenpeißenberg ozone sonde before 6:00 CET is, thus, fortuitous. ~~Different air masses must be assumed at~~
 269 ~~different altitudes. At different altitudes different air components~~ must be assumed as indicated by matching of the
 270 sonde ozone with lidar measurements at different times. ~~The spatial and temporal requirements for comparisons~~
 271 ~~can be even of the order of 1 km and 15 min at times (see Introduction).~~

272 ~~Until 2010 the lidar results were routinely compared with the long-term measurements at Wank and Zugspitze.~~
 273 ~~Apart from occasional orographically induced deviations an agreement to within ± 2 ppb was found. After these~~
 274 ~~in-situ measurements were terminated we have routinely compared the lidar measurements with the ozone~~
 275 ~~measurements at UFS. Mostly a similar agreement is found.~~

276 3.1 Comparisons of the IFU ozone lidar and the Jülich ECC sonde

277 An optimum lidar validation became possible in early 2019. On 5 and 6 February 2019 a side-by-side instrument
 278 comparison took place at Garmisch-Partenkirchen as a contribution to the FIRMOSOS (~~Far-Infrared Radiation~~
 279 ~~Mobile Observation System~~) validation project of the European Space Agency (~~Palehetti et al., 2021; Di Natale~~
 280 ~~et al., 2021~~). Two of the three balloons launched on 5 February were equipped with ozone sondes, while both
 281 balloons on 6 February carried an ozone sonde. The ascents took place during night-time because of comparisons
 282 of the CFH sondes with the water-vapour channel of the UFS Raman lidar that provides humidity profiles up to
 283 at least 20 km (Klanner et al. 2021).

284 The first night of the campaign was clearer. The conditions for the comparison were excellent: the sondes rose
285 almost vertically up to 8.5 km and then slowly drifted to the south-east (Innsbruck), ideal for the tropospheric
286 comparison. The balloons stayed within 20 km distance from IMK-IFU up to the tropopause (12.8 km a.s.l.) and
287 remained within 30 km up to 20 km a.s.l.

288 The launch times of the balloons were 18:03 CET (ascent to 16.147 km), 19:03 CET (29.475 km), and 23:00
289 CET (29.469 km).

290 In Fig. 2 we present the results of the four comparisons made. The measurements of lidar, ECC sonde and in-situ
291 sensor at UFS on 5 and 6 February are in outstanding agreement provided that a correction of a small constant
292 altitude-independent positive offset (not shown) is applied to the (uncalibrated) sonde ozone between -0.53 and
293 -3.4 ppb for the first three comparisons. The DIAL measurements are smoothed with a numerical filter with an
294 interval width growing with altitude (Trickl et al., 2020a). Nevertheless we are highly content that the
295 agreement stays exceptional towards the tropopause even in the upper troposphere is exceptional considering the
296 low differential absorption for the wavelength pair 292 nm – 313 nm typically used above 6 km that implies a
297 high sensitivity to potential technical imperfection.

298 In addition, we show in Fig. 2 the results of three humidity measurements with the UFS Raman lidar slightly
299 revised with respect to (Klanner et al. (2021) at a distance of 9 km from IMK-IFU. For comparison, we added
300 the water-vapour mixing ratios (MRs) for the corresponding CFH sonde ascents of FZJ. The water-vapour
301 mixing ratios (MR) MRs indicate a high variability of the air composition between up to 7 km on both days, up to
302 7 km, with a series several of rapidly changing dry layers. The variability grows with time, as can also be
303 concluded from the differences of Raman lidar and CFH sonde, caused by the 1-h measurement duration of the
304 lidar needed for good stratospheric data quality. In this altitude range the MR do not agree quantitatively with
305 those obtained with the CFH sondes. The MR of the lidar is much less modulated because of the 1 h data-
306 acquisition time necessary for the stratosphere. Although the vertical concentration change is much less
307 pronounced in the ozone profiles, it is obvious because of this variability that the excellent a good air-mass
308 matching by the side-by-side ozone soundings at IMK-IFU is crucial for the quality of the comparison
309 achieved results.

310 On 6 February the quality of the lidar retrievals was deteriorated by a layer of cirrus clouds above 9 km, which
311 required an aerosol correction. An increased level of ozone in this layer is remarkable, but is verified by the
312 sonde. By contrast, Reichardt et al. (1996) reported full ozone depletion in a cirrus layer that we traced back to
313 the surface of the Pacific Ocean where ozone destruction can be assumed to prevail (Kley et al., 1996). The
314 fourth comparison shows less perfect agreement because the lidar measurements ended at 19:00 CET, hours
315 before the last sonde ascent. This was the final measurement of the DIAL before its operation was terminated
316 after almost three decades.

317 Ozone profiles are also available for the descent of the balloons. The descents took place over Northern Italy and
318 intersected different air masses. As a consequence, strong discrepancies are seen, and we do not include these
319 data.

320 For quantifying the quality of the lidar measurements we took just the first three comparisons yield average
321 deviations of the sonde from the lidar. In order to evaluate the agreement of the vertical profiles of the two
322 systems in structure we determined the the average sonde offsets, determined up to 5.8 about 6 km (i.e. in the
323 range of the best lidar performance), yielding values between +0.53 and +3.4 ppb. These offsets were first
324 subtracted from the sonde ozone values profiles. Then, the differences between the corrected sonde and the lidar
325 data were formed at intervals of 52.5 m, for the first comparison on 6 February just up to 8.7 km. Finally, we

Trupdwlhu#kuliw@u#kuvly

326 averaged these differences (Fig. 3). The ~~agreement between the two systems without the single measurement~~
327 ~~offsets differences~~ -up to 9.2 km ~~stay within~~ ± 2.5 ppb (about ± 5 %). This is ~~also approximately~~ the ~~agreement~~
328 ~~performance we have found between the lidar and the mountain stations carefully evaluated over the many~~
329 years ~~by comparison with the mountain stations and, thus,~~ characterizes the winter-time ~~performance~~
330 ~~specifications~~ of the lidar after 2011. ~~This result justifies to use the lidar as a quality standard in the comparisons~~
331 ~~with the MOHp Brewer-Mast sondes described in the following sections.~~

332 The quality of the comparison shown in this section benefits from low to moderate ozone densities during the
333 cold season, which ensures limited absorption of the laser radiation within the troposphere. In Sect. 3.2 we assess
334 the performance for all seasons.

335 3.2 Comparison of MOHp ozone soundings with IFU lidar and in-situ measurements for 2018

336 The routine measurements with the IFU ozone DIAL exhibit rather different annual coverages, with gaps due to
337 system damage or upgrading periods. Starting in late 2012 the final technical performance was reached.
338 Retrieval strategies have been further improved. The best coverage of a single year was achieved in 2018 with a
339 total of 587 measurements and 16 (March) to 79 (September) measurements per month. Therefore, we use this
340 year for a thorough comparison with the MOHp ozone sonde.

341 The sonde ascents at MOHp usually take place around 6:00 CET on Monday, Wednesday and Friday, in summer
342 just on Monday and Wednesday. We found a total of 46 of these days on which early-morning lidar
343 measurements exist, not later than around 10:00 CET. On 36 of these days MOHp soundings are available.
344 Thirteen of the days provided particularly good conditions with favourable temporal proximity. In the figures
345 shown in this paper we eliminate ozone profiles for times later than 10:00 CET during a given day.

346 *Winter*

347 During the cold parts of the year the comparisons usually exhibit better quality. This is explained by less
348 structured ~~in the~~ ozone vertical distributions and a wider operating range of the lidar due to the low ozone level
349 allowing for a higher, less noisy far-field signal. This was already demonstrated in the previous section. For the
350 2018 comparison we give one example in Fig. 4. The lidar mixing ratio is of the order of 45 ppb, verified by the
351 measurements at UFS (2660 m a.s.l.). ~~There is an obvious constant offset of the sonde mixing ratio with respect~~
352 ~~to the lidar ozone profile. After adding 5.8 ppb~~ The sonde results (*cyan curve*) match the lidar values well
353 ~~above 2.1 km if one adds 5.8 ppb~~. Just below the tropopause there is a minor discrepancy that could be either due
354 to the higher uncertainty of the lidar measurement at these altitudes or air-mass differences.

355 *Summer*

356 During the warm season the ozone distribution in the middle and upper troposphere shows structured maxima
357 caused by long-range transport, in particular STT (stratosphere-to-tropopause transport) layers (Trickl et al.,
358 2020b). In this altitude range a summer maximum of STT exists. Usually, these structures do not perfectly match
359 for both sites. An example for 9 July 2018 is shown in Fig. 5.

360 Figure 5 shows good agreement in structure between the soundings at both sites up to 9 km, in the presence of
361 northerly advection. Again, ~~despite the pronounced ozone layering,~~ the agreement was improved on the absolute
362 scale by adding an ~~altitude-independent~~ correction to the sonde values (6 ppb). ~~Thus, this approach was applied~~
363 ~~throughout our study. The offset is usually determined up to 6 km due to the reliable performance of the 277-nm-~~

Irupdwlhu@i.fk#Chuyrukheq

Irupdwlhu@i.fk#Chuyrukheq

Irupdwlhu@i.fk#Chuyrukheq

364 ~~313-nm measurements, but the agreement is mostly reasonable also to higher altitudes. After shifting the sonde~~
365 ~~mixing ratio we can estimate the uncertainty of the lidar measurements.~~

366 The elevated ozone between 3.3 km and 4.7 km can be explained by a stratospheric air intrusion, as is verified by
367 the low RH. In the upper troposphere the agreement deteriorates, but at least the increase of ozone with altitude
368 is seen in all profiles up to about 12 km. The ozone minimum around 13 km is just seen in the lidar data, with
369 just a small ozone dip in the sonde profile. It is unreasonable to ascribe this considerable discrepancy to a
370 temporary technical problem in such a limited altitude range. This example documents the difficulty of
371 quantitative comparisons of tropospheric ozone even on a horizontal scale of just 38 km.

372 In order to clarify the origin of the difference of the ozone mixing ratio in the upper troposphere we calculated
373 backward trajectories with the HYSPLIT model (<http://ready.arl.noaa.gov/HYSPLIT.php>; Draxler and Hess,
374 1998; Stein et al., 2015). These trajectories ~~reveal northerly advection which implies a southward drift of the~~
375 ~~sonde towards the lidar during the ascent. In the upper troposphere they did not fully explain the observations~~
376 ~~due to within~~ the limited maximum backward time span of 315 h. This includes “ensemble” trajectory bundles
377 that visualize a wider range of source regions.

378 Therefore, the trajectory calculations were extended to 350 h by using the LAGRANTO model for full-hour start
379 times between 3:00 CET and 8:00 CET, ~~initiated in the low-ozone range in the upper troposphere.~~ Results for
380 start times of 7:00 CET and 8:00 CET are shown in Figs. 6 and 7. Up to a start time of 4:00 CET the trajectories
381 stayed almost completely at high altitudes. At 5:00 CET three of the trajectories ended in the lower troposphere
382 above the subtropical Pacific near a longitude of 180°, first sign of an air-mass change. Later (Figs. 6 and 7) we
383 see a clear influence of a Pacific source.

384 The low ozone level in the boundary layer above (sub)tropical oceans is well known (Eisele et al., 1999; Grant et
385 al., 2000; Trickl et al., 2003), in particular over the Pacific (Kley et al., 1996; Davies et al., 1998). In this way,
386 the lidar observations on 9 July 2018 can be understood. The launch time of the MOHp ozone sonde, 5:42 CET,
387 is between the two lidar measurements. However, a delay is caused ~~by the northerly advection during the ascent~~
388 ~~which makes a quantitative understanding difficult.~~

389 The moderate sonde RH ~~above 12.3 km~~ indicates a potential admixture of aged stratospheric air ~~in this altitude~~
390 ~~range~~ above MOHp which would explain the high ozone mixing ratios of more than 120 ppb.

391 Figures 5 and 8 show a rather constant negative ozone offset of the sonde profiles. The ozone profiles can be
392 brought into much better agreement by upward shifts by 6 ppb and 10 ppb, respectively. In Fig. 9 one sees one of
393 the very rare cases of ~~an clear~~-ozone mismatch between sonde and lidar up to elevations clearly above the
394 mountain sites (1 km above the Zugspitze summit). ~~We did not shift the MOHp profile (e.g., by 3 ppb) to reduce~~
395 ~~the mismatch since this would reduce the good agreement above 4 km.~~

396 ~~We conclude that differences between the Zugspitze sites and the MOHp sonde are mostly not related to~~
397 ~~differences in air composition in contrast to what was suspected earlier.~~

398 Offsets

399 The offsets of the MOHp data ~~from the DIAL profiles~~ were evaluated for all 36 comparison days. The result ~~of~~
400 ~~the statistical assessment~~ is displayed in Fig. 10 where also the differences between the lidar results for 2671 m
401 a.s.l. and the GAW measurements at UFS are shown. ~~Just one case was eliminated: A strong negative shift of -7~~
402 ~~ppb can be seen in Fig. 5 where UFS is located in the falling edge of a high-ozone range~~

Irupdwlu#evwdqgru##5\$w1d/fk##3\$w1/
]hlohqdevwd#qidf

Irupdwlu#fkuliw@lw#xuvl#fkuliwidueh=
Dxwrpdwlvfk

403 As found for the lidar measurements over many years (examples: Trickl et al., 2014, 2015, 2016, 2020b) the
404 lidar ozone agrees with that at UFS to within ± 3 ppb. The agreement would perhaps be better if orographic
405 vertical displacements and air flows on the ozone profiles would be considered (Carnuth et al., 2000; 2002; Yuan
406 et al., 2019; Trickl et al., 2020a). ~~Orographic effects matter particularly in summer. Under warm conditions the
407 lidar ozone seems to be slightly higher on average with respect to UFS. A strong negative shift of -7 ppb can be
408 seen in Fig. 5 where UFS is located in the falling edge of a high ozone range. This case was discarded from the
409 statistical assessment.~~

410 The average difference between lidar and UFS for 2018 (blue horizontal line in Fig. 10) is $0.736 \text{ ppb} \pm 1.46 \text{ ppb}$
411 (standard deviation). A positive offset had also been found for an earlier four-day comparison with the Zugspitze
412 summit, but with even higher uncertainty (Trickl et al., 2020a). A positive offset of this size could be expected
413 from the highly accurate cross-section measurements of Viallon et al. (2015), who determined a negative bias of
414 1.8% of the in-situ data calibrated with the WMO standard. This relative difference becomes more important on
415 the absolute scale in summer than in winter because of the higher ozone values. ~~It might explain the slight
416 seasonal cycle of the difference visible in Fig. 10. However, given the complex orography at the site we
417 think~~ However, that the ~~uncertainties~~ statistical noise of the differences ~~are~~ is too high for such a conclusion to
418 allow resolving such an effect.

419 The offsets between the MOHp sonde and the lidar are substantially higher (red filled squares in Fig. 10). We
420 ~~exclude the lowest altitudes from the comparison where obvious differences in ozone exist, e.g., due to local
421 night time ozone depletion effects. The offsets of the ozone sondes range from -12 ppb to +4 ppb, with an
422 average of -3.77 ppb (red horizontal line in Fig. 10) and a standard deviation of 4.22 ppb.~~

423 ~~The comparisons with the Zugspitze summit are mostly reasonable. We exclude the lowest altitudes from the
424 comparison where obvious differences in ozone exist, e.g., due to local night-time ozone depletion effects. It is
425 important to note that~~ just in seven cases of the 36 comparisons for 2018 lower ozone in the sonde profiles
426 reached up to more than 2.67 km (UFS), in three cases to more than 3 km (Zugspitze summit). We conclude that
427 differences between the Zugspitze sites and the MOHp sonde are mostly related to sonde calibration issues and
428 not to differences in air composition as suspected earlier.

429 ~~The offsets of the ozone sondes range from -12 ppb to +4 ppb, with an average of -3.77 ppb and a standard
430 deviation of 4.22 ppb.~~

431 **Differences**

432 ~~In order to determine the quality of the lidar measurements we show~~ ~~In~~ ~~in~~ the three panels of Figs. 11 to 13 we
433 ~~show~~ average differences between lidar and offset-corrected MOHp sonde data as a function of altitude and for
434 three different ozone conditions, roughly below 50 ppb (low ozone), between 50 to 70 ppb (moderate ozone) and
435 more than 70 ppb (high ozone). ~~The averaging was carried out just for measurement days with lidar
436 measurements in temporal proximity to the launch time of the ozone sonde. On a given day, the lidar ozone
437 profiles agreeing best with the MOPp profile was taken.~~ We also give the percentages of the averages with
438 respect to the offset-corrected sonde ozone. At high altitudes the sonde ozone is a more useful reference than the
439 lidar in the case of high ozone because of the considerable absolute uncertainty caused by the loss of laser
440 radiation by absorption.

441 For winter-type conditions ("low ozone": mixing ratio mostly less than 50 ppb; top panel) the six examples
442 averaged do not exhibit low a significant vertical ozone structure which made the analysis straight forward and
443 yields astonishingly small average differences between ± 1 ppb and ± 3 ppb. For moderate ozone (second panel)

IrupdwluWkuliw@LkXuvly

444 and high ozone (bottom panel), mostly during the warm season, the vertical distributions are more complex with
445 changes on a time scale of even less than one hour. Here, we eliminated ~~the data several for a few obvious~~
446 ~~pronounced~~ ozone peaks and dips that differed at both stations. The six high-ozone cases were restricted to July
447 and August.

448 The averaged distributions of the differences exhibit oscillations. These oscillations were analysed for coherency
449 (not shown), but no systematic behaviour was identified. Thus, we ascribe the structure to noise. The noise
450 contains both an atmospheric and an instrumental component.

451 ~~The noise amplitude shrinks above 6 km because of the change from 277 nm as the “on” wavelength to 292 nm.~~
452 ~~This step is not clearly seen in Fig. 13 due to the higher 292 nm noise level. Beyond the days and years of the~~
453 ~~comparison In July and August there are occasionally extreme cases with 100 to 150 ppb in the middle and upper~~
454 ~~troposphere. This can lead to lidar uncertainties even up to more than 20 ppb during day-time, also because of~~
455 ~~the raw signal becomes comparable with the additional solar background noise. This is larger than the excursions~~
456 ~~in the average in Fig. 13. In the severest cases the stratospheric ozone rise cannot be seen in the lidar data during~~
457 ~~daytime, and the ozone profile is cut off in the upper troposphere for archiving.~~

458 The analyses for 2018 do not reveal a significant bias between the lidar values and the offset-corrected sonde
459 data (based on the numbers underlying Fig. 10). The maximum noise excursions can be interpreted as maximum
460 combined uncertainties of lidar and corrected sonde in a given altitude range. The results of this analysis confirm
461 the estimates in Table 4 of Trickl et al. (2020a).

462 3.3 Comparisons of MOHp sonde, IFU lidar and in-situ measurements at summits in 2009

463 The results in Sect. 3.2 suggested to look also at a few earlier years. We select 2009 from the period of routine
464 measurements as another year of comparison. The lidar raw data were noisier than for the period after 2012 and
465 a tiny electronic ringing effect had to be removed mathematically. Thus, the uncertainties of the ozone profiles
466 above 6 km are higher than after the final system upgrading in 2012, particularly in summer. As a consequence,
467 a lidar validation is desirable at least for the upper troposphere. More importantly, in 2009 high-quality ozone
468 data still exist for the summit stations Wank (1780 m a.s.l.) and Zugspitze (2962 m a.s.l.). These stations benefit
469 from more frequent direct advection compared with UFS.

470 In 2009 the lidar was operated just until October which, nevertheless, allows us to make a reasonable number of
471 comparisons with MOHp. The operation was stopped afterwards since there were more and more cases of single-
472 bit errors in channel 5 of the transient digitizer system which had to be sent for repair. These errors induced
473 unrealistic data in the upper troposphere.

474 We identified a total of 23 days suitable for comparisons. On just eight of these days lidar measurements were
475 made in optimum temporal proximity. We find more deviations in the profiles than for 2018. In part, this can be
476 explained by atmospheric variability and insufficient air-mass matching. In addition, as mentioned, the raw data
477 of the lidar are noisier and some weak ringing had to be removed. This caused elevated uncertainties above 6
478 km. Nevertheless, the data allowed us to determine offsets for the MOHp ozone profiles, after verifying the data
479 quality of the lidar with the Zugspitze and Wank in-situ ozone.

480 In Fig. 14-12 we show the results of the analysis for 2009. The difference between IFU DIAL and Zugspitze is
481 $-0.165 \text{ ppb} \pm 1.36 \text{ ppb}$ (standard deviation), between DIAL and Wank $+0.714 \text{ ppb} \pm 1.20 \text{ ppb}$. The DIAL ozone
482 below the Wank altitude is increasingly uncertain because of alignment issues of the near-field telescope. In an
483 earlier comparison for May 1999 (Trickl et al., 2020a) we selected a lower altitude in the DIAL data (2786 m)

IrupdlhuWkuliw@uEcWxuvly

IrupdlhuWkuliw@uEcWxuvly

484 and found better agreement, but, still, a slight positive offset with respect to the station. This is not attempted
485 here, although we can see the effect of orographic lifting in some examples.
486 For 2009 the offsets between DIAL and MOHp sondes were determined primarily by between 2 and 5 km. The
487 sonde offset obtained in this way is, again, negative on average (-1.500 ppb), with a standard deviation of 2.67
488 ppb, both being are less pronounced than in 2018.

489 Figure 15-13 shows a comparison on 12 January 2009, demonstrating excellent agreement between both
490 systems, except for the upper troposphere and lower stratosphere. In this case, the first lidar measurement took
491 place at 9:20 CET, i.e., substantially later than the sonde ascent. Thus, the comparison has its limits. In the
492 morning of 12 January westerly advection was revealed by HYSPLIT backward trajectories above at 7 km a.s.l..
493 This air mass originated below 2 km over the subtropical Atlantic. This could explain the slightly lower ozone
494 level around this altitude in the lidar results.

495 Another interesting example is August 17 (Fig. 1614). The agreement between lidar and ozone sonde is highly
496 satisfactory up to 5.4 km and quite reasonable up to 10 km. However, between 10 km and 14.5 km the lidar
497 ozone is extremely low, in contrast to the sonde data. The pronounced ozone increase in the sonde data above 10
498 km is difficult to explain since the elevated RH values suggest neither a low tropopause nor the presence of a
499 stratospheric intrusion that typically features RH values of a few per cent at most (Trickl et al., 2014; 2015;
500 2016). On the other hand, the ozone peak above IMK-IFU descending roughly from 10 to 8 km is attributed by
501 HYSPLIT calculations to subsiding air, indicating the presence of an intrusion layer. It is interesting that the
502 rather short delay of the lidar measurements (7:00 CET to 9:15 CET) with respect to the sonde ascent (launch
503 time 5:57 CET) can result in such a considerable difference.

504 Again, 350-h LAGRANTO trajectories were calculated for start times above IMK-IFU between 3:00 CET and
505 8:00 CET (interval: 1 h) and start altitudes within the low-ozone layer. Until 6:00 CET the influence of marine
506 boundary layers is almost absent. Afterwards, the trajectories reveal a growing import from the first 600 m above
507 the subtropical Atlantic Ocean. In Fig. 17-15 the LAGRANTO results for 8:00 CET are shown.

508 In many cases the lidar seems to exhibit a negative bias with respect to the sondes in the upper troposphere. It is
509 advisable to re-examine a major part of the data between 2007 and 2011, also including strategies developed
510 later. For example, an exponential decay of the analogue signal was identified with the much lower noise of the
511 final setup (Trickl et al., 2020a) which must be addressed.

512 3.4 Comparisons of MOHp sonde, IFU lidar and in-situ measurements summits in 2000 and 2001

513 The period September 2000 to August 2001 is suitable for another comparison when a large number of STT-
514 related measurement series were made as a contribution to the STACCATO project (Stohl et al., 2003;
515 examples: Trickl et al., 2003; 2010; 2011; Zanis et al., 2003). These measurements were made with the noisier
516 detection electronics of Eisele et al. (1999), but had the advantage that single-photon counting was used for the
517 “solar blind” “on” detection channels which added linearity above 5 km (starting in spring 1997). The counting
518 system was abandoned could no longer be computer controlled after 2003/2006. A new one was installed after
519 highly positive results in other IFU lidar systems in 2018 (Klanner et al., 2021) in autumn 2018, too late for
520 routine operation this comparison effort.

521 The focus on STT during the STACCATO period made the comparisons a challenge because of the pronounced
522 layering. However, on 11 of the useful 20 days of comparison there was reasonable temporal proximity, due to
523 running long time series. The agreement between the lidar and the MOHp sonde was much better than expected
524 in the entire free troposphere. The agreement (after offset-correcting the MOHp profiles) is almost perfect during

Trupdwlhuv#kuliw@lckwxyly

525 the cold season. But also under high-ozone conditions the comparisons do not reveal systematic differences
526 beyond the sonde offsets.

527 Two examples for elevated ozone are shown in Figs. 18-16 and 19-17. The good comparisons support our earlier
528 work (Trickl et al., 2003, and 2010, respectively), and we tend to ascribe this to the good-satisfactory
529 performance of the single-photon counting system.

530 For several weeks a strange ozone rise towards the ground was observed in the lidar data below 1.5 km. This
531 effect disappeared after realigning the near-field telescope and the normal early-morning ozone drop returned.

532 However, the offsets of the MOHp mixing ratios necessary to achieve good agreement are, again, quite
533 substantial (Fig. 20-18). Due to the larger system noise during that period aAlso the differences between lidar and
534 the stations are higher than those in the preceding sections, and comparable with those of the mentioned four-day
535 comparison for May 1999 (Trickl et al., 2020a). The statistical analysis yields the following average differences
536 and standard deviations:

537 IFU DIAL – Zugspitze: 1.22 ppb ± 1.81 ppb

538 IFU DIAL – Wank -0.15 ppb ± 2.26 ppb

539 MOHp – IFU DIAL -5.88 ppb ± 3.35 ppb

540 4. Discussion and Conclusions

541 For some time tropospheric differential-absorption ozone lidar systems had a bad reputation: The method is
542 highly sensitive to imperfections in the signal acquisition since the ozone number density is obtained by
543 derivative formation differentiating the backscatter signals. In addition, a lidar covering the entire troposphere
544 and the lowermost stratosphere features a dynamic range of the backscatter signal of about eight decades, which
545 means an extreme challenge for the detection electronics.

546 Based on continual improvements, starting with the 1994 system upgrading, the IFU ozone DIAL gradually
547 approached a high performance until 2012, but there is, still, minor potential for improvements remains.
548 Comparison with the nearby mountain stations quite early demonstrated an uncertainty level of ±3 ppb in the
549 lower troposphere. Occasional comparisons with ozone sondes launched at the Hohenpeißenberg (1996 to 2001,
550 distance 38 km) were rather satisfactory up to the tropopause region.

551 Here, we more comprehensively we analyse the lidar performance in three periods during its technical
552 development analyse the lidar performance during three periods in its technical development in a more
553 comprehensive manner. The best agreement was found for the side-by-side comparison with balloon ascents of
554 ozone sondes, performed by the FZJ team at IMK-IFU in February 2019. Just a small, constant offset had to be
555 subtracted from the sonde data to achieve perfect agreement. The lidar itself agreed with the three local summit
556 stations. For all three years and all stations we determined a positive bias of just 0.6 ppb ± 0.6 ppb. This seems to
557 reflect the -1.8-% calibration deficit of the WMO calibration of the in-situ ozone data. Thus, the lidar could be
558 even free of bias in the lower free troposphere.

559 -For the more distant MOHp sonde the comparisons are more demanding because of the high atmospheric
560 variability (Vogelmann et al., 2011; 2015). This variability is particularly severe in summer when the
561 atmospheric layering is more pronounced. Nevertheless, there was enough agreement in certain altitude ranges
562 for examining the reliability of the ozone profiles obtained from the DIAL, also before the final modifications in
563 2012. It turned out that justBetween 2007 and 2011 we can-suspect a slight negative summertime bias of the
564 lidar of the order of 5 ppb above 6 km (not quantified because of insufficient data). This could be due to
565 interfering structures on the 292-nm analogue signal (requiring mathematical correction) that could not be

Irupdlhu#kuliw#B#wl#fk#xuvly

Irupdlhu#kuliw#B#wl

566 compensated by photon counting (available ~~just~~ until 2003) ~~and daylight-induced signal distortions at 313 nm~~
567 (Trickl et al., 2020a). In principle, this calls for a re-evaluation of the ozone profiles ~~for the wavelength pair 292~~
568 ~~nm - 313 nm~~ over the period 2007 to 2011, based on more recent experience in the signal inversion and the
569 performance of the electronic equipment.

570 Vice versa, the lidar measurements helped us to ~~identify-validate~~ the quality of the sonde measurements. Quite
571 good agreement ~~can-could~~ be achieved by applying an altitude-independent offset correction to the ozone values
572 that strongly varies from sonde to sonde. ~~In all but a few cases the offset can be determined to within ±2 ppb by~~
573 ~~a comparison with the Zugspitze or the UFS station data.~~ Most of the ~~timeozone~~-differences ~~in-early-morning~~
574 ~~air-mass-composition-between~~ the two sites are limited to altitudes below 2 km. Thus, the differences reported
575 earlier by Scheel for 3 km (see introduction) are not caused by ~~systematic~~ differences in air composition at both
576 sites. ~~As can be seen from the figures presented in this paper the shifted sonde and the Zugspitze ozone mostly~~
577 ~~agrees to within ±3 ppb. Given the frequently substantially higher ozone offsets of the MOHp sondes. A~~
578 ~~recalibration of the archived sonde data based on~~ comparisons with the ~~Zugspitze or UFS~~ in-situ data is
579 advisable despite the considerable distance between the sites. ~~Such a recalibration should be avoided in the~~
580 ~~presence of pronounced ozone structure around the station altitudes which could be accounted for by elevated~~
581 ~~uncertainties.~~

582 The comparisons for the three years 2000-2001, 2009 and 2018 reveal just minor performance change of the
583 MOHp sonde over the years, with a variation of the annual average offset by about ±2 ppb. We found a negative
584 average offset of $-3.64 \text{ ppb} \pm 3.72 \text{ ppb}$ (standard deviation) with respect to the IFU ozone DIAL over all three
585 years. It is reasonable to assume that this offset is applicable to the entire tropospheric time series of the MOHp
586 sondes.

587 Remaining tasks for the lidar are a substantial reduction of the solar background at 313.2 nm in summer and to
588 enhance the moderate 291.8-nm backscatter signal in the upper troposphere. Further reduction of the residual
589 solar background is difficult since the spectral filtering is already quite narrow. However, replacement of the
590 rather aged (and partly contaminated) primary mirror of the far-field receiver could help by reducing the
591 background radiation reflected into the detection system. As mentioned longer averaging is advisable. By longer
592 averaging, the performance under low-aerosol conditions could almost reach that of ~~in-situ measurements in a~~
593 major part of the troposphere. Single-photon counting can also be helpful for longer averaging times, as
594 demonstrated for our Raman lidar (Klanner et al., 2021). The noise level for counting is still lower than that of
595 the meanwhile outstanding transient digitizers (Trickl et al., 2020a).

596 5 Data availability

597 Lidar data and information on the lidar systems can be obtained on request from the IMK-IFU authors of this
598 paper (thomas@trickl.de, hannes.vogelmann@kit.edu). The 313-nm aerosol backscatter coefficients are archived
599 in the EARLINET data base, accessible through the ACTRIS data portal <http://actris.nilu.no/>. The
600 Hohenpeißenberg ozone and humidity data are stored in the NDACC data archive ([https://www-](https://www-air.larc.nasa.gov/missions/ndacc/data.html#)
601 [air.larc.nasa.gov/missions/ndacc/data.html#](https://www-air.larc.nasa.gov/missions/ndacc/data.html#)). The data of the FIRMOS campaign is available via the ESA
602 campaign dataset website <https://earth.esa.int/eogateway/campaigns/firmos>. ~~The hourly Zugspitze and UFS~~
603 ~~ozone data are available at the World Data Center for Reactive Gases (WDCRG: <https://ebas.nilu.no/>) and the~~
604 ~~TOAR data base (Schultz et al., 2017).~~

605 6 Author statement

606 TT carried out most lidar measurements after spring 1997, following U. Kempfer and H. Eisele. He led the
607 technical development of two ozone DIAL systems since 1990. HV was involved in the system upgrading since
608 2007 and was responsible for the lidar operation during FIRMOS. DC and CW launched several ECC sondes at
609 IMK-IFU in February 2019. MA and WS carried out the MOHP ozone sonde measurements. LR performed
610 ~~Ozone-ozone~~ in-situ measurements at ~~the site Schneefernerhaus~~UFS. MS provided LAGRANTO backward
611 trajectories.

Irupdwlhuv#kuliw@l#kwxvly

612 7 Competing interests

613 The authors declare that they have no conflict of interest.

614 Acknowledgements

615 The authors thank Wolfgang Seiler and Hans Peter Schmid for their support over so many years. The late Hans-
616 Eckhart Scheel provided reference ozone data for the Wank, Zugspitze and ~~Schneefernerhaus~~ mountain stations
617 in the vicinity of IMK-IFU. The different steps of lidar development have been funded by the German Ministry
618 of Research and Technology (BMFT), the German Foundation for the Environment (DBU, two projects), and the
619 Bavarian Ministry of Economics. Since 2007 the 313-nm aerosol results have contributed to EARLINET
620 (European Aerosol Research Lidar Network) that is currently a part of the European Research Infrastructure
621 ACTRIS (Aerosol, Clouds and Trace Gases Research Infrastructure). The lidar measurements were also funded
622 by the European Union within Vertical Ozone Transport 1 and 2 (e.g., Wotava, G., and Kromp-Kolb, 2000;
623 VOTALP 2, 2000) and STACCATO (Stohl et al., 2003) and by the German Ministry for Research and
624 Education (BMBF) within ATMOfAST (2005).

625 KIT acknowledges support of lidar measurements by the European Space Agency (ESA) under Contract
626 4000123691/18/NL/NF (FIRMOS validation campaign). Balloon profiles utilized in this paper have been
627 provided within the same ESA project by the Forschungszentrum Jülich via subcontract with KIT. The balloon
628 activities were also partly supported by the Helmholtz Association in the framework of MOSES (Modular
629 Observation Solutions for Earth Systems).

630 The service charges for this open access publication have been covered by a Research Centre of the Helmholtz
631 Association.

632 References

633 ATMOfAST: Atmosphärischer Ferntransport und seine Auswirkungen auf die Spurengaskonzentrationen in der
634 freien Troposphäre über Mitteleuropa (Atmospheric Long-range Transport and its Impact on the Trace-gas
635 Composition of the Free Troposphere over Central Europe), Project Final Report, T. Trickl, co-ordinator, M.
636 Kerschgens, A. Stohl, and T. Trickl, subproject co-ordinators, funded by the German Ministry of Education and
637 Research within the programme “Atmosphärenforschung 2000“, <http://www.trickl.de/ATMOfAST.htm>, 130
638 pp., 2005 (in German), with revised publication list of 2012

639 Ancellet, G., Pelon, J., Beekmann, M., Papayannis, A., and Mégie, G.: Ground-Based Lidar Studies of Ozone
640 Exchanges Between the Stratosphere and the Troposphere, *J. Geophys. Res.*, 96, 22401-22421, 1991.

641 Ancellet, G., Godin-Beekmann, S., Smit, H. G. J., Stauffer, R. M., Van Malderen, R., Bodichon, R., and
642 Pazmiño, A.: Homogenization of the Observatoire de Haute Provence electrochemical concentration cell (ECC)
643 ozonesonde data record: comparison with lidar and satellite observations, *Atmos. Meas. Tech.*, 15, 3105–3120,
644 2022.

645 Attmannspacher, W., and Dütsch, H.: 2nd International Ozone Sonde Intercomparison at the Observatory of
646 Hohenpeissenberg, *Berichte des Deutschen Wetterdienstes* 157, 1981.

647 Beekmann, M., Ancellet, G., Mégie, G., Snit, H. G. J., and Kley, D.: Intercomparison Campaign of Vertical
648 Ozone Profiles Including Electrochemical Sondes of ECC and Brewer-Mast Type and a Ground Based UV-
649 Differential Absorption Lidar, *J. Atmos. Chem.*, 19, 259-288, 1994.

650 [Belotti, C., Barbara, F., Barucci, M., Bianchini, G., D'Amato, F., Del Bianco, S., Di Natale, G., Gai, M.,
651 Montori, A., Pratesi, F., Rolf, C., Sussmann, R., Trickl, T., Viciani, S., Vogelmann, H., Palchetti, L.: The Far-
652 Infrared Radiation Mobile Observation System for spectral characterisation of the atmospheric emission, *Atmos.
653 Meas. Tech.*, 16, 2511–2529, <https://doi.org/10.5194/amt-16-2511-2023>.](#)

654 Brabec, M.: Backscatter and Humidity Measurements in Cirrus and Dust Clouds using Balloon Sondes, Ph.D.
655 thesis, Eidgenössische Technische Hochschule, Zürich (Switzerland), 96 pp., 2011.

656 Brewer, A. W., and Milford, J. R.: The Oxford-Kew ozone sonde, *Proc. R. Soc. Lond. A*, 256, 470–495
657 [available at <http://doi.org/10.1098/rspa.1960.0120>], 1960.

658 Browell, E. V., Danielsen, E. F., Ismail, S., Gregory, G. L., and Beck, S. M.: Tropopause Fold Structure
659 Determined From Airborne Lidar and in Situ Measurements, *J. Geophys. Res.*, 92, 2112-2120, 1987.

660 Carnuth, W., and Trickl, T.: Transport studies with the IFU three-wavelength aerosol lidar during the VOTALP
661 Mesolcina experiment, *Atmos. Environ.*, 34, 1425-1434, 2000.

662 Carnuth, W., Kempfer, U., and Trickl, T.: Highlights of the tropospheric lidar studies at IFU within the TOR
663 project, *Tellus B*, 54, 163-185, 2002.

664 Claude, H., Hartmannsgruber, R., and Köhler, U.: Measurement of atmospheric profiles using the Brewer-Mast
665 sonde, World Meteorological Organization, Global Ozone Res. and Monit. Proj. Report No. 17, WMO/TD No.
666 179, Geneva (Switzerland), [see also https://library.wmo.int/index.php?lvl=notice_display&id=11215], 51 pp.,
667 1987.

668 Deshler, T., Stübi, R., Schmidlin, F. J., Mercer, J. L., Smit, H. G. J., Johnson, B. J., Kivi, K., and Nardi, B.:
669 Methods to homogenize electrochemical concentration cell (ECC) ozonesonde measurements across changes in
670 sensing solution concentration or ozonesonde manufacturer, *Atmos. Meas. Tech.*, 10, 2021–2043, 2017.

671 Daumont, D., Brion, J., Charbonnier, J., and Malicet, J.: Ozone UV Spectroscopy I: Absorption Cross-Sections
672 at Room Temperature, *J. Atmos. Chem.*, 15, 145-155, 1992.

673 Davies, W. E., Vaughan, G., and O'Connor, F. M.: Observation of near-zero ozone concentrations in the upper
674 troposphere at mid-latitudes, *Geophys. Res. Lett.*, 25, 1173-1176, 1998.

675 De Backer, H., De Muer, D., and De Sadelaeer G.: Comparison of ozone profiles obtained with Brewer-Mast and
676 Z-ECC sensors during simultaneous ascents, *J. Geophys. Res.*, 103, 19,641–19,648,
677 <https://doi.org/10.1029/98JD01711> , 1998.

678 De Muer, D., and Malcorps, H.: The frequency response of an electrochemical ozone sonde and its application to
679 the deconvolution of ozone profiles, *J. Geophys. Res.*, 89, 1361–1372, 1984.

680 Di Natale, G., Barucci, M., Belotti, C., Bianchini, G., D'Amato, F., Del Bianco, S. Gai, M., Montori, A.,
681 Sussmann, R., Viciani, S., Vogelmann, H., and Palchetti, L.: Comparison of mid-latitude single- and mixed-

Trupdwlu#kuliw@khw

Trupdwlu#ejolv#huhqlj#vqljuhlfk,

682 phase cloud optical depth from co-located infrared spectrometer and backscatter lidar measurements, *Atmos.*
683 *Meas. Tech.*, 14, 6749–6758, 2021.

684 Dirksen, R. J., Sommer, M., Immler, F. J., Hurst, D. F., Kivi, R., and Vömel, H.: Reference quality upper-air
685 measurements: GRUAN data processing for the Vaisala RS92 radiosonde, *Atmos. Meas. Tech.*, 7, 4463–4490,
686 doi.org/10.5194/amt-7-4463-2014, 2014.

687 Draxler, R., and Hess, G.: An overview of the HYSPLIT_4 modelling system for trajectories, dispersion, and
688 deposition, *Aust. Meteorol. Mag.*, 47, pp. 295–308, 1998.

689 Eisele, H., Trickl, T., and Claude, H.: Lidar als wichtige Ergänzung zur Messung troposphärischen Ozons,
690 *Ozonbulletin des Deutsches Wetterdiensts*, 44, 2 pp., 1997 (in German).

691 Eisele, H., Scheel, H. E., Sladkovic, R., and Trickl, T.: High-Resolution Lidar Measurements of Stratosphere-
692 Troposphere Exchange, *J. Atmos. Sci.*, 56, 319–330, 1999.

693 Eisele, H., and Trickl, T.: Improvements of the aerosol algorithm in ozone-lidar data processing by use of
694 evolutionary strategies, *Appl. Opt.*, 44, 2638–2651, 2005.

695 EUROTRAC: Transport and Chemical Transformation of Pollutants in the Troposphere, Vol. 1, An Overview of
696 the Work of EUROTRAC, P. Borrell and P. M. Borrell, Eds., Springer (Berlin, Heidelberg, New York), ISBN 3-
697 540-66775-X, 474 pp., 1997.

698 Gaudel, A., Ancellet G., and Godin-Beckmann S.: Analysis of 20 years of tropospheric ozone vertical profiles by
699 lidar and ECC at Observatoire de Haute Provence (OHP) at 44° N, 6.7° E, *Atmos. Environ.*, 113, 78–89, 2015.

700 Gaudel, A., Cooper, O. R., Ancellet, G., Barret, B., Boynard, A., Burrows, J. P., Clerbaux, J. P., Coheur, P.-F.,
701 Cuesta, J., Cuevas, E., Doniki, S., Dufour, G., Ebojic, F., Foret, G., Garcia, O., Granados-Muñoz, M. J.,
702 Hannigan, J., Hase, F., Hassler, B., Huang, G., Hurtmans, D., Jaffé, D., Jones, N., Kalabokas, P., Kerridge, B.,
703 Kulawik, S., Latter, B., Leblanc, T., Le Flochmoën, E., Lin, W., Liu, J., Liu, X., Mahieu, E., McClure-Begley,
704 A., Neu, J., Osman, M., Palm, M., Petetin, H., Petropavlovskikh, I., Querel, R., Raupach, N., Rozanov, A.,
705 Schultz, M. G., Schwab, J., Siddans, R., Smale, D., Steinbacher, M., Tanimoto, H., Tarasick, D., Thouret, V.,
706 Thompson, A., M., Trickl, T., Weatherhead, E., Wespes, C., Worden, H., Vigouroux, C., Xu, X., Zeng, G.,
707 Ziemke, J.: Tropospheric Ozone Assessment Report: Present-day distribution and trends of tropospheric ozone
708 relevant to climate and global atmospheric chemistry model evaluation, *Elem. Sci. Anth.*, 6, 39, DOI:
709 <https://doi.org/10.1525/elementa.291>, 58 pp., 2018.

710 Grant, W. B., Browell, E. V., Butler, C. F., Fenn, M. A., Clayton, M. B., Hannan, J. R., Fuelberg, H. E., Blake,
711 D. R., Blake, N. J., Gregory, G. L., Heikes, B. G., Sachse, G. W., Singh, H. B., Snow, J., and Talbot, R. W.: A
712 case study of transport of tropical marine boundary layer and lower tropospheric air masses to the northern
713 midlatitude upper troposphere, *J. Geophys. Res.*, 105, 3757–3769, 2000.

714 Hearn, A. G.: The Absorption of Ozone in the Ultra-violet and Visible Regions of the Spectrum, *Proc. Phys.*
715 *Soc.*, 78, 932–940, 1961.

716 Hersbach, H., Bell, B., Berrisford, P., Simmons, A., Berrisford, P., Dahlgren, P., Horanyi, A., Muñoz-Sabater, J.,
717 Nicolas, J., Radu, R., Schepers, D., Soci, C., Villaume, S., Bidlot, J. R., Haimberger, L.; Woollen, J.,
718 Buontempo, C., and Thepaut, J. N.: The ERA5 global reanalysis. *Q. J. R. Meteorol. Soc.*, 146, 1999– 2049,
719 <https://doi.org/10.1002/qj.3803>, 2020.

720 Johnson, B. J., Oltmans, S. J., Vömel, H., Smit, H. G. J., Deshler, T., and Kröger, C.: Electrochemical
721 concentration cell (ECC) ozonesonde pump efficiency measurements and tests on the sensitivity to ozone of
722 buffered and unbuffered ECC sensor cathode solutions, *J. Geophys. Res.-Atmos.*, 107, ACH 8-1–ACH 8-18,
723 <https://doi.org/10.1029/2001JD000557>, 2002.

724 Jeannot, P., Stübi, R., Levrat, G., Viatte, P., and J. Staehelin, J.: Ozone balloon soundings at Payerne
725 (Switzerland): Reevaluation of the time series 1967–2002 and trend analysis, *J. Geophys. Res.*, 112, D11302,
726 doi:10.1029/2005JD006862, 15 pp., 2007.

727 Kempfer, U., Carnuth, W., Lotz, R., and Trickl, T.: A wide range ultraviolet lidar system for tropospheric ozone
728 measurements: development and application, *Rev. Sci. Instrum.*, 65, 3145-3164, 1994.

729 Kerr, J. B., Fast, H., McElroy, C.T., Oltmans, S.J., Lathrop, J.A., Kyro, E., Paukkunen, A., Claude, H., Köhler,
730 U., Sreedharan, C.R., akao T., and Tsukagoshi, Y.: The 1991 WMO International Ozonesonde Intercomparison
731 at Vanskoj, Canada. *Atmos.–Ocean*, 32, 685–716, <https://doi.org/10.1080/07055900.1994.9649518>, 1994.

732 Klanner, L., Höveler, K., Khordakova, D., Perfahl, M., Rolf, C., Trickl, T., and Vogelmann, H.: A powerful lidar
733 system capable of 1 h measurements of water vapour in the troposphere and the lower stratosphere as well as the
734 temperature in the upper stratosphere and mesosphere, *Atmos. Meas. Tech.*, 14, 531-555, 2021.

735 Klausen, J., Zellweger, C., Buchmann, B., and Hofer, P.: Uncertainty and bias of surface ozone measurements at
736 selected Global Atmospheric Watch sites, *J. Geophys. Res.*, 108, 4622, doi: 10.1029/2003JD003710, 17 pp.,
737 2003.

738 Kley, D., Beck, J., Grennfelt, P. I., Hov, O., and Penkett, S. A.: Tropospheric Ozone Research (TOR) A Sub-
739 Project of EUROTRAC, *J. Atmos. Chem.*, 28, 1–9, 1997.

740 Kley, D., Crutzen, P. J., Smit, H. G. J., Vömel, H., Oltmans, S., Grassl, H., and Ramanathan, V.: Observations of
741 Near-Zero Ozone Concentrations Over the Convective Pacific: Effects on Air Chemistry, *Science*, 274, 230-233,
742 1996.

743 Komhyr, W.D.: Electrochemical concentration cells for gas analysis, *Ann. Geoph.*, 25, 203–210, 1969.

744 Komhyr, W. D., Barnes, R. A., Brothers, G. B., Lathrop, J. A., and Opperman, D. P.: Electrochemical
745 concentration cell ozonesonde performance evaluation during STOIC 1989, *J. Geophys. Res.*, 100, 9231–9244,
746 <https://doi.org/10.1029/94JD02175>, 1995.

747 Langford, A. O., Masters, C. D., Proffitt, M. H., Hsie, E.-Y., and Tuck, A. F.: Ozone measurements in a
748 tropopause fold associated with a cut-off low system, *Geophys. Res. Lett.*, 23, 2501–2504, 1996.

749 Logan, J.A., Staehelin, J., Megretskaia, I.A., Cammas, J.-P., Thouret, V., Claude, H., De Backer, H.,
750 Steinbacher, M., Scheel, H.-E., Stübi, R., Fröhlich, M., and Derwent, R. (2012), Changes in ozone over Europe:
751 Analysis of ozone measurements from sondes, regular aircraft (MOZAIC) and alpine surface sites, *J. Geophys.*
752 *Res.*, 117, D09301, doi:10.1029/2011JD016952.

753 Malicet, J., Daumont, D., Charbonnier, J., Parisse, C., Chakir, A., and Brion, J.: Ozone UV Spectroscopy I:
754 Absorption Cross-Sections and Temperature Dependence, *J. Atmos. Chem.*, 21, 263-273, 1995.

755 Palchetti, L., Barucci, M., Belotti, C., Bianchini, G., Cluzet, B., D'Amato, F., Del Bianco, S., Di Natale, G., Gai,
756 M., Khordakova, D., Montori, A., Oetjen, H., Rettinger, M., Rolf, C., Schuettemeyer, D., Sussmann, R., Viciani,
757 S., Vogelmann, H., and Wienhold, F. G.: Observations of the downwelling far-infrared atmospheric emission at

758 the Zugspitze observatory, *Earth Syst. Sci. Data*, 13, 4303–4312, <https://doi.org/10.5194/essd-13-4303-2021>,
759 2021.

760 [Parrish, D. D., Derwent, R. G., Steinbrecht, W., Stübi, R., Van Malderen, R., Steinbacher, M., Trickl, T., Ries,](#)
761 [L., and Xu, X.: Zonal Similarity of Long-term Changes and Seasonal Cycles of Baseline Ozone at Northern](#)
762 [Mid-latitudes. *J. Geophys. Res.*, 125, e2019JD031908, <https://doi.org/10.1029/2019JD031908>, 19 pp., 2020.](#)

763 Schultz, M. G., Schröder, S., Lyapina, O., Cooper, O., Galbally, I., Petropavlovskikh, I., von Schneidmesser,
764 E., Tanimoto, H., Elshorbany, Y., Naja, M., Seguel, R. J., Dauert, U., Eckhardt, P., Feigenspan, S., Fiebig, M.,
765 Hjellbrekke, A.-G., Hong, Y.-D., Kjeld, P. C., Koide, H., Lear, G., Tarasick, D., Ueno, M., Wallasch, M.,
766 Baumgardner, D., Chuang, M.-T., Gillett, R., Lee, M., Molloy, S., Moolla, R., Wang, T., Sharps, K., Adame, J.
767 A., Ancellet, G., Apadula, F., Artaxo, P., Barlasina, M. E., Bogucka, M., Bonasoni, P., Chang, L., Colomb, A.,
768 Cuevas-Agulló, E., Cupeiro, M., Degorska, A., Ding, A., Fröhlich, M., Frolova, M., Gadhavi, H., Gheusi, F.,
769 Gilge, S., Gonzalez, M. Y., Gros, V., Hamad, S. H., Helmig, D., Henriques, D., Hermansen, O., Holla, R.,
770 Hueber, J., Im, U., Jaffe, D. A., Komala, N., Kubistin, D., Lam, K.-S., Laurila, T., Lee, H., Levy, I., Mazzoleni,
771 C., Mazzoleni, L. R., McClure-Begley, A., Mohamad, M., Murovec, M., Navarro-Comas, M., Nicodim, F.,
772 Parrish, D., Read, K. A., Reid, N., Ries, L., Saxena, P., Schwab, J. J., Scorgie, Y., Senik, I., Simmonds, P.,
773 Sinha, V., Skorokhod, A. I., Spain, G., Spangl, W., Spoor, R., Springston, S. R., Steer, K., Steinbacher, M.,
774 Suharguniyawan, E., Torre, P., Trickl, T., Weili, L., Weller, R., Xiaobin, X., Xue, L., and Zhiqiang, M.:
775 Tropospheric Ozone Assessment Report: Database and Metrics Data of Global Surface Ozone Observations,
776 *Elem. Sci. Anth.*, 5, 58, DOI: <https://doi.org/10.1525/elementa.244>, 25 pp., 2017.

777 Reichardt, J., Ansmann, A., Serwazi, M., Weitkamp, C., and Michaelis, W.: Unexpectedly low ozone
778 concentration in midlatitude tropospheric ice clouds: A case study, *Geophys. Res. Lett.*, 23, 1929–1932, 1996.

779 Smit, H. G. J., Straeter, W., Johnson, B. J., Oltmans, S. J., Davies, J., Tarasick, D. W., Hoegger, B., Stubi, R.,
780 Schmidlin, F. J., Northam, T., Thompson, A. M., Witte, J. C., Boyd, I., and Posny, F.: Assessment of the
781 Performance of ECC-ozonesondes under Quasi-flight Conditions in the Environmental Simulation Chamber:
782 Insights from the Jülich Ozone Sonde Intercomparison Experiment (JOSIE), *J. Geophys. Res.*, 112, D19306,
783 doi:10.1029/2006JD007308, 18 pp., 2007.

784 Smit, H.G.J., and ASOPOS panel: Quality assurance and quality control for ozonesonde measurements in GAW,
785 World Meteorological Organization, GAW Report No. 201, Geneva (Switzerland). [Available online at
786 https://library.wmo.int/doc_num.php?explnum_id=7167], 100 pp., 2014.

787 Smit, H.G.J., and Thompson, A.M.: Ozonesonde Measurement Principles and Best Operational Practices:
788 ASOPOS 2.0 (Assessment of Standard Operating Procedures for Ozonesondes), World Meteorological
789 Organization, GAW Report No. 268, Geneva (Switzerland). [Available online at
790 https://library.wmo.int/doc_num.php?explnum_id=10884], 172 pp., 2021.

791 Stauffer, R.M., Thompson, A.M., Kollonige, D.E., Tarasick, D.W., Van Malderen, R., Smit, H.G.J., Vömel, H.,
792 Morris, G.A., Johnson, B.J., Cullis, P.D., Stübi, R., Davies, J., and Yan.: An Examination of the Recent Stability
793 of Ozonesonde Global Network Data, *Earth and Space Science*, 9 (10), e2022EA002459, [available online at
794 <https://doi.org/10.1029/2022EA002459>], 2022.

795 Stein, A. F., Draxler, R. R., Rolph, G. D., Stunder, B. J. B., Cohen, M. D., and Ngan, F.: NOAA's HYSPLIT
796 atmospheric transport and dispersion modeling system, *Bull. Amer. Meteor. Soc.*, 96, 2059–2077, 2015.

Trupdwluh#f#kuliw#B#w#f#qjolv#f#zhuhlgjwhv
N`qljuhlfk,

797 Steinbrecht, W., Schwarz, R., and Claude, H.: New pump correction for the Brewer-Mast ozone sonde:
798 determination from experiment and instrument intercomparisons, *J. Atmos. Ocean. Tech.*, 15, 144–156, 1998.

799 Stohl, A., and Trickl, T.: A textbook example of long-range transport: Simultaneous observation of ozone
800 maxima of stratospheric and North American origin in the free troposphere over Europe, *J. Geophys. Res.*, 104,
801 30445–30462, 1999.

802 Stohl, A., Bonasoni, P., Cristofanelli, P., Collins, W., Feichter, J., Frank, A., Forster, C., Gerasopoulos, E.,
803 Gäggeler, H., James, P., Kentarchos, T., Kromp-Kolb, H., Krüger, B., Land, C., Meloen, J., Papayannis, A.,
804 Priller, A., Seibert, P., Sprenger, M., Roelofs, G. J., Scheel, H. E., Schnabel, C., Siegmund, P., Tobler, L., Trickl,
805 T., Wernli, H., Wirth, V., Zanis, P., and Zerefos, C.: Stratosphere-troposphere exchange - a review, and what we
806 have learned from STACCATO, *J. Geophys. Res.*, 108, 8516, doi:10.1029/2002JD002490, STA 1, 15 pp., 2003.

807 Stübi, R., Levrat, G., Hoegger, B., Pierre Viatte, P., Staehelin, J., Schmidlin, F.J.: In-flight comparison of
808 Brewer-Mast and electrochemical concentration cell ozonesondes, *J. Geophys. Res.*, 113, D13302,
809 <https://doi.org/10.1029/2007JD009091>, 2008.

810 Tarasick, D. W., Davies, J., Anlauf, K., Watt, M., Steinbrecht, W., Claude H.-J.: Laboratory investigations of the
811 response of Brewer-Mast ozonesondes to tropospheric ozone, *J. Geophys. Res.*, 107, ACH 14-1 – 14-10,
812 <https://doi.org/10.1029/2001JD001167>, 2002.

813 Tarasick, D. W., Davies, J., Smit, H. G. J., and Oltmans, S. J.: A re-evaluated Canadian ozonesonde record:
814 measurements of the vertical distribution of ozone over Canada from 1966 to 2013, *Atmos. Meas. Tech.*, 9, 195–
815 214, <https://doi.org/10.5194/amt-9-195-2016>, 2016.

816 Tarasick, D., Galbally, I. E., Cooper, O. R., Schultz, G. M., Ancellet, G., Leblanc, T., Wallington, T. J., Ziemke,
817 J., Liu, X., Steinbacher, M., Staehelin, J., Vigouroux, C., Hannigan, J., Garcia, O., Foret, G., Zanis, P.,
818 Weatherhead, E., Petropavlovskikh, I., Worden, H., Osman, M., Liu, J., Chang, K.-L., Gaudel, A., Lin, M.,
819 Granados-Muñoz, M., Thompson, A. M., Oltmans, S. J., Cuesta, J., Dufour, G., Thouret, V., Hassler, B., Trickl,
820 T., and Neu, J. L.: Tropospheric Ozone Assessment Report: Tropospheric ozone from 1877 to 2016, observed
821 levels, trends and uncertainties, *Elem. Sci. Anth.*, 7, Article 39, DOI: <https://doi.org/10.1525/elementa.376>, 72
822 pp. (plus 56 pp. of supplemental material), 2019.

823 Tarasick, D. W., Smit, H. G. J., Thompson, A. M., Morris, G. A., Witte, J. C., Davies, J., Davies, J., Nakano, T.,
824 Van Malderen, R., Stauffer, R. M., Johnson, B. J., Stubi1, R., Oltmans, S. J., and Vömel, H.: Improving ECC
825 ozonesonde data quality: Assessment of current methods and outstanding issues, *Earth and Space Science*, 8,
826 e2019EA000914. <https://doi.org/10.1029/2019EA000914>, 27 pp., 2021.

827 TESLAS: Tropospheric Environmental Studies by Laser Sounding (TESLAS), in: *Transport and Chemical*
828 *Transformation of Pollutants in the Troposphere*, Vol. 8, Instrument Development for Atmospheric Research and
829 Monitoring, J. Bösenberg, D. Brassington, and P. C. Simon, Eds., Springer (Berlin, Heidelberg, New York),
830 ISBN 3-540-62516-X, 1-203, 1997.

831 Thompson, A. M., Smit, H. G. J., Witte, J. C., Stauffer, R. M., Johnson, B. J., Morris, G., von der Gathen, P.,
832 Van Malderen, R., Davies, J., Piters, A., Allaart, M., Posny, F., Kivi, R., Cullis, P., Hoang Anh, N. T., Corrales,
833 E., Machinini, T., da Silva, F. R., Paiman, G., Thiong’o, K., Zainal, Z., Brothers, G. B., Wolff, K. R., Nakano,
834 T., Stübi, R., Romanens, G., Coetzee, G. J. R., Diaz, J. A., Mitro, S., Mohamad, M., and Ogino, S.: Ozonesonde
835 Quality Assurance: The JOSIE–SHADOZ (2017) Experience, *Bulletin of the American Meteorological Society*,
836 100, 155-171, 2019.

837 Trickl, T., Cooper, O. R., Eisele, H., James, P., Mücke, R., and Stohl, A.: Intercontinental transport and its
838 influence on the ozone concentrations over central Europe: Three case studies, *J. Geophys. Res.*, 108, D12, 8530,
839 10.1029/2002JD002735, *STA* 15, 23 pp., 2003.

840 Trickl, T., Feldmann, H., Kanter, H.-J., Scheel, H. E., Sprenger, M., Stohl, A., and Wernli, H.: Deep
841 stratospheric intrusions over Central Europe: case studies and climatological aspects, *Atmos. Chem. Phys.*, 10,
842 499-524, 2010.

843 Trickl, T., Eisele, H., Bärtsch-Ritter, N., Furger, M., Mücke, R., Sprenger, M., and Stohl, A.: High-ozone layers
844 in the middle and upper troposphere above Central Europe: potential import from the stratosphere along the
845 subtropical jet stream, *Atmos. Chem. Phys.*, 11, 9343-9366; 5-p. Supplement, 2011.

846 Trickl, T., Vogelmann, H., Giehl, H., Scheel, H. E., Sprenger, M., and Stohl, A.: How stratospheric are deep
847 stratospheric intrusions? *Atmos. Chem. Phys.*, 14, 9941-9961, 2014.

848 Trickl, T., Vogelmann, H., Flentje, H., and Ries, L.: Stratospheric ozone in boreal fire plumes – the 2013 smoke
849 season over Central Europe, *Atmos. Chem. Phys.*, 15, 9631-9649, 2015.

850 Trickl, T., Vogelmann, H., Fix, A., Schäfler, A., Wirth, M., Calpini, B., Levrat, G., Romanens, G., Apituley, A.,
851 Wilson, K. M., Begbie, R., Reichardt, J., Vömel, H. and Sprenger, M.: How stratospheric are deep stratospheric
852 intrusions into the troposphere? LUAMI 2008, *Atmos. Chem. Phys.*, 16, 8791-8815, 2016.

853 Trickl, T., Neidl, F., Giehl, H., Perfahl, M., and Vogelmann, H.: Three decades of tropospheric ozone lidar
854 development at Garmisch-Partenkirchen, *Atmos. Meas. Tech.*, 13, 6357-6390, 2020a.

855 Trickl, T., Vogelmann, H., Ries, L., and Sprenger, M.: Very high stratospheric influence observed in the free
856 troposphere over the Northern Alps – just a local phenomenon? *Atmos. Chem. Phys.*, 20, 243-266, 2020b.

857 Trickl, T., Couret, C., Ries, L., and Vogelmann, H.: Zugspitze ozone 1978 – 2020: The role of stratosphere-
858 troposphere transport, *Atmos. Chem. Phys.*, ACP-2022-783, under final review (2023)

859 Vaisala: Vaisala Radiosonde RS41 Measurement Performance, White Paper, Vaisala, Helsinki (Finland),
860 [https://www.vaisala.com/sites/default/files/documents/WEA-MET-RS41-Performance-White-paper-](https://www.vaisala.com/sites/default/files/documents/WEA-MET-RS41-Performance-White-paper-B211356EN-B-LOW-v3.pdf)
861 [B211356EN-B-LOW-v3.pdf](https://www.vaisala.com/sites/default/files/documents/WEA-MET-RS41-Performance-White-paper-B211356EN-B-LOW-v3.pdf), 28 pp. (accessed 7 September 2019), 2017.

862 Van Malderen, R., Allaart, M. A. F., De Backer, H., Smit, H. G. J., and De Muer, D.: On instrumental errors and
863 related correction strategies of ozonesondes: possible effect on calculated ozone trends for the nearby sites Uccle
864 and De Bilt, *Atmos. Meas. Tech.*, 9, 3793–3816, 2016

865 Viallon, J., Lee, S., Moussay, P., Tworek, K., Peterson, M., and Wielgosz, R. I.: Accurate measurements of
866 ozone absorption cross-sections in the Hartley band, *Atmos. Meas. Tech.*, 8, 1245-1257, 2015.

867 Völger, P., Bösenberg, J., and Schult, I.: Scattering Properties of Selected Model Aerosols Calculated at UV-
868 Wavelengths: Implications for DIAL Measurements of Tropospheric Ozone, *Beitr. Phys. Atmosph.*, 69, 177-
869 187, 1996.

870 Vömel, H., David, D. E., and Smith, K.: Accuracy of tropospheric and stratospheric water vapor measurements
871 by the cryogenic frost point hygrometer: Instrumental details and observations, *J. Geophys. Res.*, 112, D08305,
872 doi: 10.1029/2006JD007224, 14 pp., 2007.

873 Vömel, H., Naebert, T., Dirksen, R., and Sommer, M.: An update on the uncertainties of water vapor
874 measurements using Cryogenic Frostpoint Hygrometers, *Atmos. Meas. Tech.*, 9, 3755-3768, 2016.

Irupdwlhu#ejolv#xhuhlqlj#ivljuhlfk,
Irupdwlhu#ejolv#xhuhlqlj#ivljuhlfk,

875 Vömel, H., Smit, H. G. J., Tarasick, D., Johnson, B., Oltmans, S. J., Selkirk, H., Thompson, A. M., Stauffer, R.
876 M., Witte, J. C., Davies, J., van Malderen, R., Morris, G. A., Nakano, T., and Stübi, R.: A new method to correct
877 the electrochemical concentration cell (ECC) ozonesonde time response and its implications for “background
878 current” and pump efficiency, *Atmos. Meas. Tech.*, 13, 5667–5680, 2020.

879 Vogelmann, H. and Trickl, T.: Wide-Range Sounding of Free-Tropospheric Water Vapor with a Differential-
880 Absorption Lidar (DIAL) at a High-Altitude Station, *Appl. Opt.*, 47, 2116-2132, 2008.

881 Vogelmann, H., Sussmann, R., Trickl, T., and Borsdorff, T.: Intercomparison of atmospheric water vapor
882 soundings from the differential absorption lidar (DIAL) and the solar FTIR system on Mt. Zugspitze, *Atmos.*
883 *Meas. Tech.*, 4, 835-841, 2011.

884 Vogelmann, H., Sussmann, R., Trickl, T., and Reichardt, A.: Spatiotemporal variability of water vapor
885 investigated using lidar and FTIR vertical soundings above the Zugspitze, *Atmos. Chem. Phys.*, 14, 3135-3148,
886 2015.

887 VOTALP II: Vertical Ozone Transport in the Alps II, Final Report for the European Union, Contract Nr.: ENV4
888 CT970413, Reporting Period 1/3/1998-29/2/2000, H. Kromp-Kolb, Co-ordinator, Universität für Bodenkultur
889 Wien (Austria), Institut für Meteorologie und Physik, 96 pp., 2000.

890 Wernli, H., and Davies, H.C.: A Lagrangian-based analysis of extratropical cyclones. I: The method and some
891 applications. *Q.J.R. Meteorol. Soc.*, 123: 467-489, <https://doi.org/10.1002/qj.49712353811>, 1997.

892 Sprenger, M., and Wernli, H.: The LAGRANTO Lagrangian analysis tool – version 2.0, *Geosci. Model Dev.*, 8,
893 2569–2586, <https://doi.org/10.5194/gmd-8-2569-2015>, 2015.

894 Wotava, G., and Kromp-Kolb, H.: The research project VOTALP – general objectives and main results, *Atmos.*
895 *Environ.*, 34, 1319-1322, 2000.

896 Yuan, Y., Ries, L., Petermeier, H., Trickl, T., Leuchner, M., Couret, C., Sohmer, R., Meinhardt, F., and Menzel,
897 A.: On the diurnal, weekly, and seasonal cycles and annual trends in atmospheric CO₂ at Mount Zugspitze,
898 Germany, during 1981–2016, *Atmos. Chem. Phys.*, 19, 999–1012, <https://doi.org/10.5194/acp-19-999-2019>,
899 2019.

900 Zanis, P., Trickl, T., Stohl, A., Wernli, H., Cooper, O., Zerefos, C., Gaeggeler, H., Priller, A., Schnabel, C.,
901 Scheel, H. E., Kanter, H. J., Tobler, L., Kubik, P. W., Cristofanelli, P., Forster, C., James, P., Gerasopoulos, E.,
902 Delcloo, A., Papayannis, A., and Claude, H.: Forecast, observation and modelling of a deep stratospheric
903 intrusion event over Europe, *Atmos. Chem. Phys.*, 3, 763-777, 2003.

904 Zellweger, C., Buchmann, B., Klausen, J., and Hofer, P.: System and Performance Audit of Surface Ozone,
905 Carbon Monoxide and Methane at the Global GAW Station Zugspitze/Hohenpeißenberg, Platform Zugspitze,
906 Germany, Empa-WCC Report 01/1, submitted to the World Meteorological Organization, 49 pp., February
907 2001,

908 Zellweger, C., Klausen, J., and Buchmann, B.: System and Performance Audit of Surface Ozone, Carbon
909 Monoxide and Methane at the Global GAW Station Zugspitze/Schneefernerhaus, Germany, Empa-WCC Report
910 06/2, submitted to the World Meteorological Organization, 51 pp., June 2006,

911 Zellweger, C., Steinbacher, M., and Buchmann, B., and Steinbrecher, R.: System and Performance Audit of
912 Surface Ozone, Methane, Carbon Dioxide, Nitrous Oxide and Carbon Monoxide at the Global GAW Station

Irupdlhu#kuliw#B#w#qjolv#huhlqljwhv
N'qljuhlfk,

Irupdlhu#kuliw#B#w#qjolv#huhlqljwhv
N'qljuhlfk,

Irupdlhu#qjolv#huhlqljwhv#qljuhlfk,

913 [Zugspitze-Schneefernerhaus, Germany, submitted to WMO by WMO World Calibration Centre WCC-Empa](#)
914 [Empa Dübendorf, Switzerland, 46. pp., WCC-Empa Report 11/2, June 2011.](#)
915 [Zellweger, C., Steinbacher, M., Buchmann, B., and Steinbrecher, R.: System and Performance Audit of Surface](#)
916 [Ozone, Methane, Carbon Dioxide, Nitrous Oxide and Carbon Monoxide at the Global GAW Station Zugspitze-](#)
917 [Schneefernerhaus, Germany, submitted to WMO by WMO World Calibration Centre WCC-Empa Empa](#)
918 [Dübendorf, Switzerland, WCC-Empa Report 20/3, September 2020, GAW report 266, 54. pp., 2021.](#)

Irupdlhu#f#kuliw@B#W#jqjolv#k#huh1qljwhv
N`qljuhlfk,

Irupdlhu#f#kuliw@B#W#jqjolv#k#huh1qljwhv
N`qljuhlfk,

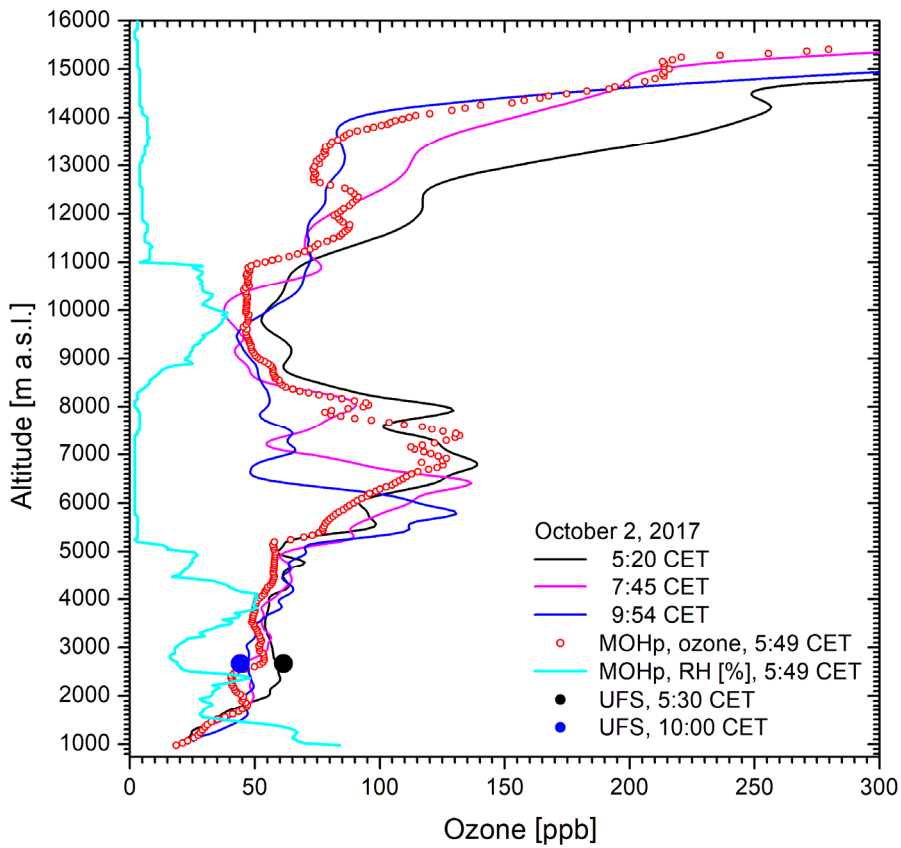
919
920

921

922 Figures:

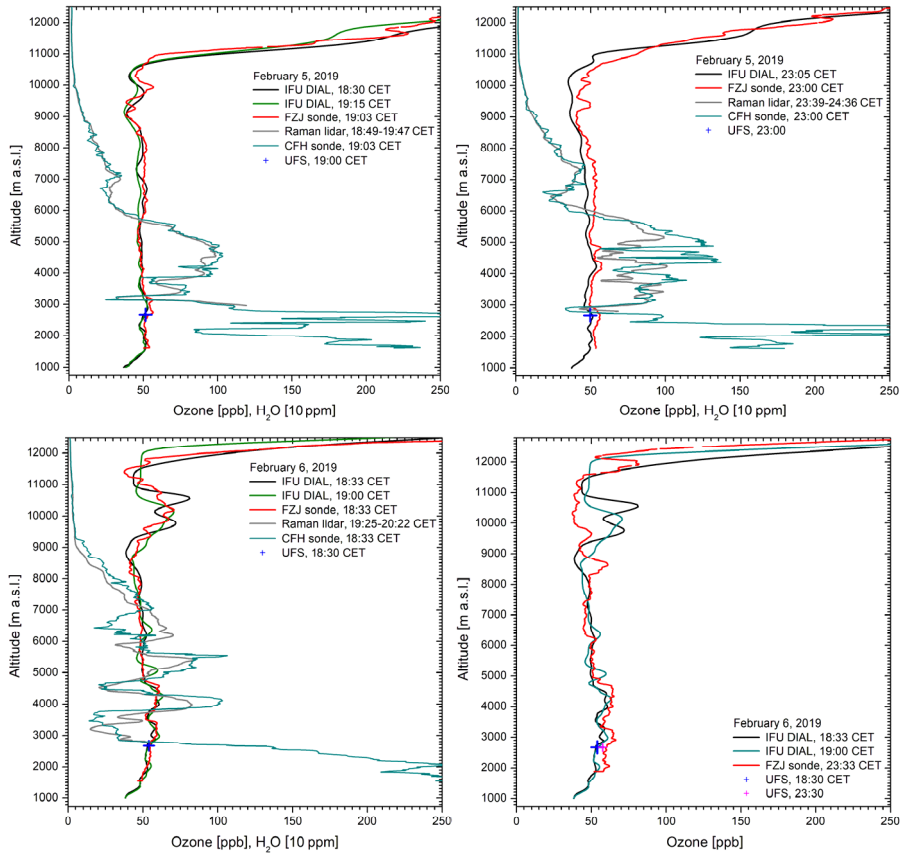
923

924



925 **Fig. 1.** Ozone measurements at Garmisch-Partenkirchen (IFU, UFS) and Hohenpeißenberg (MOHp) on 2
926 October 2017; the low relative humidity between 5.2 and 8.3 km (RH = 2 %) verifies the presence of a
927 stratospheric air intrusion. The time for MOHp is the launch time of the sonde.

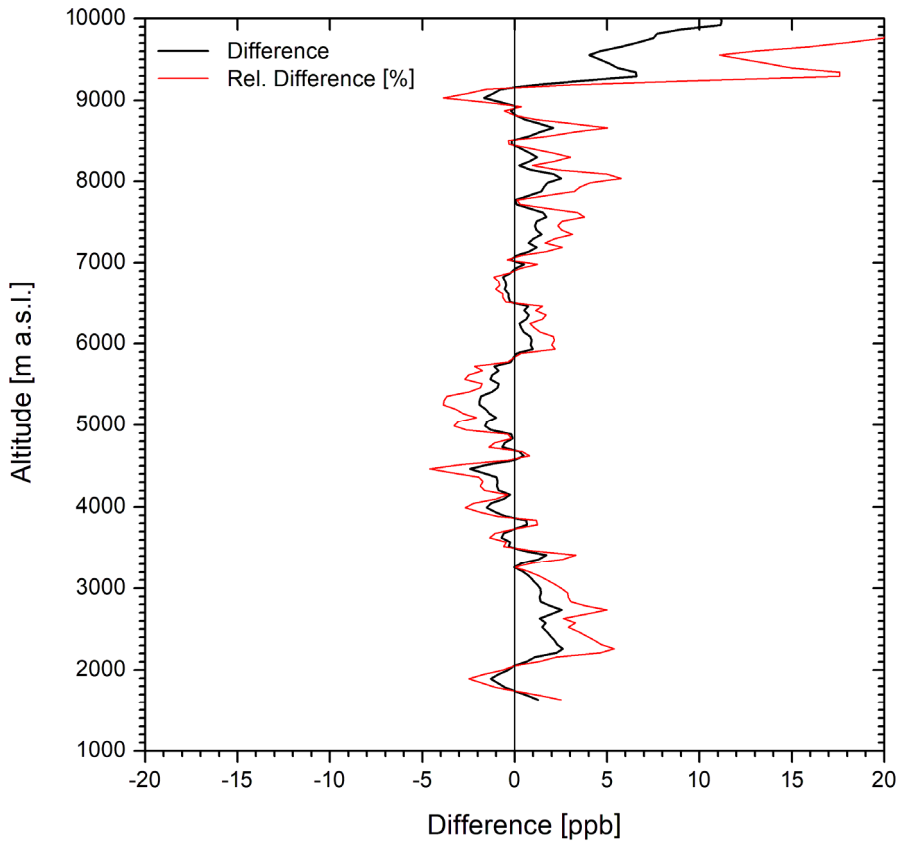
928



930 **Fig. 2.** Four ozone measurements on 5 and 6 February 2019 with lidar (IFU), ECC sonde (FZJ) and an in-situ
 931 sensor at UFS; for two measurements the FZJ ozone mixing ratios are slightly higher than the lidar results. The
 932 fourth FZJ ozone measurement took place much later than the final lidar measurements which resulted in slightly
 933 larger differences. The lidar results around 10 km on 6 February are uncertain due to a cirrus correction. In order
 934 to visualize more details on the complex layering we also show water-vapour mixing ratios for roughly co-
 935 inciding measurements of the UFS Raman lidar and the FZJ CFH sonde. The tropospheric structures are strongly
 936 smoothed for the lidar due to the 1-h data-acquisition time. At 3.3 km 250 ppm corresponds to roughly 5 % RH.
 937

Irupdwlu#kuliw@kxuvly

938

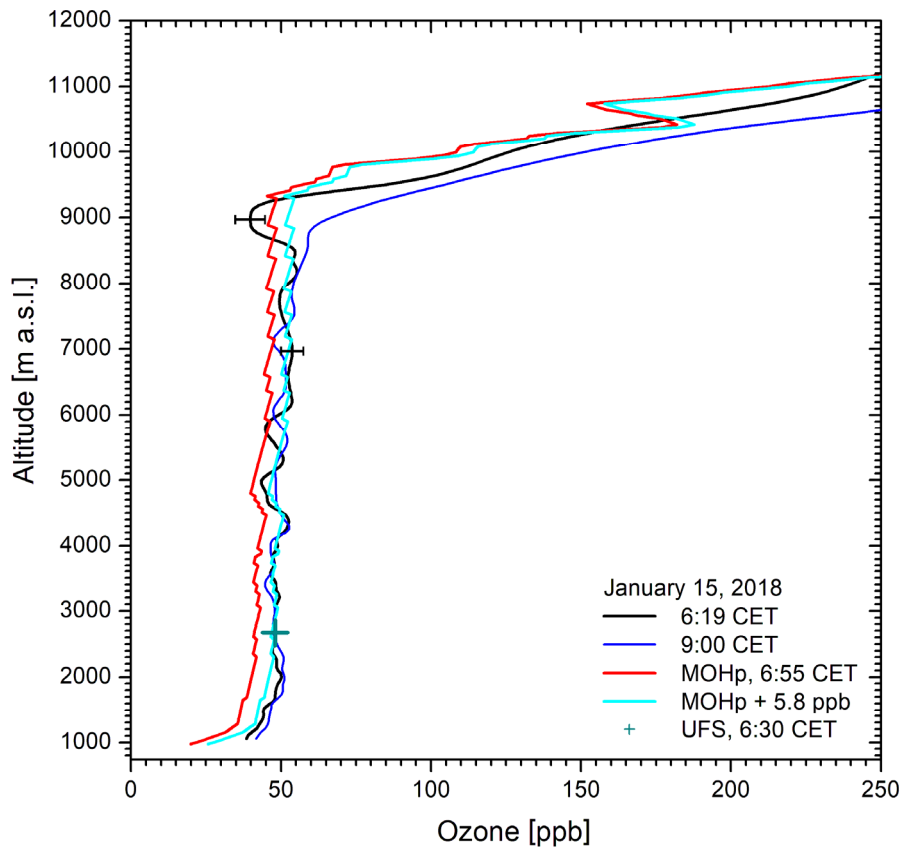


939 **Fig. 3.** Averaged differences between FZJ ozone sonde and IMK-IFU lidar for the first three comparisons after a
940 slight offset correction [of the sonde profiles](#) (see text)

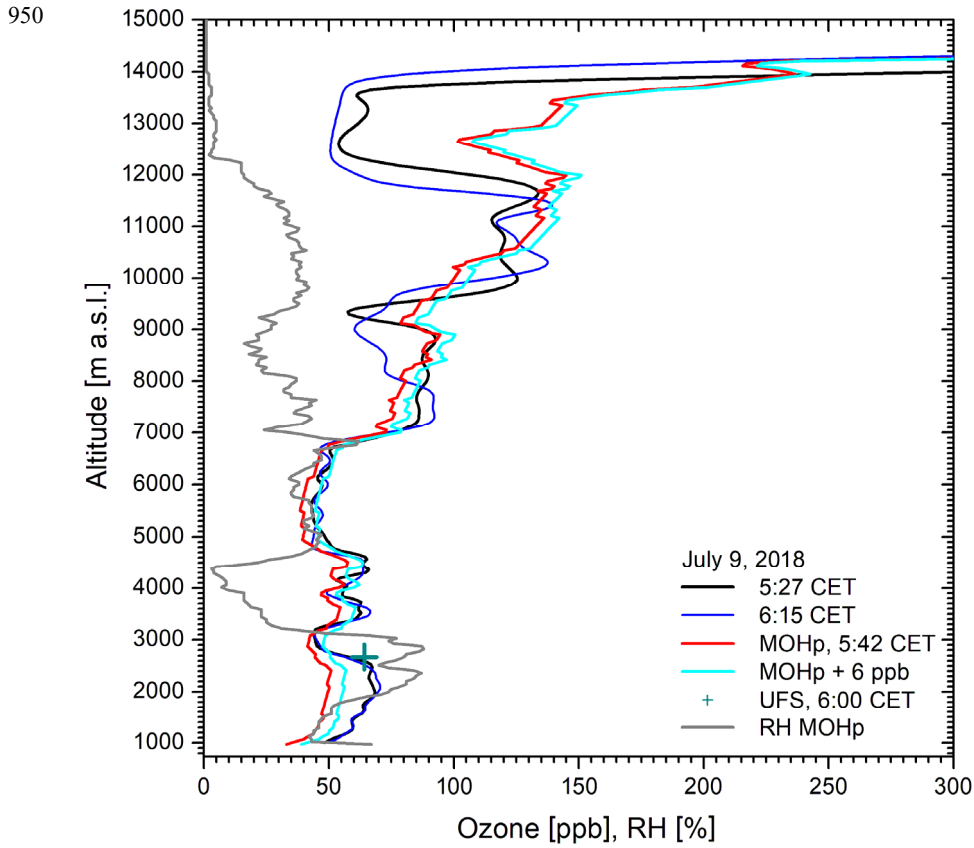
941

942

943



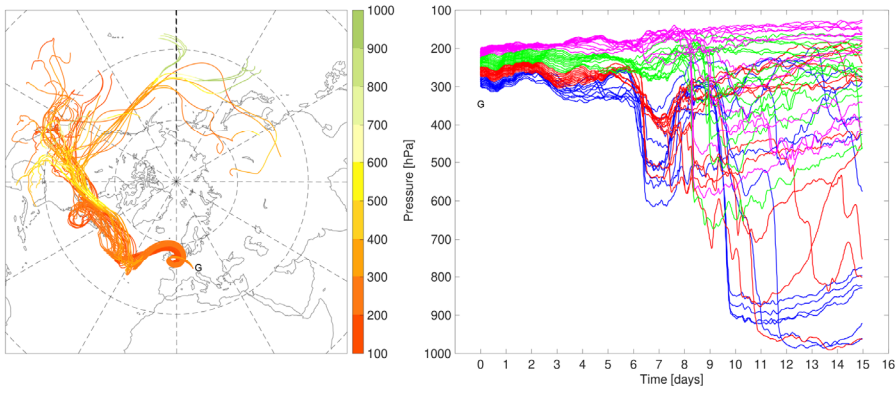
945 **Fig. 4.** Ozone measurements on 15 January 2018: The MOHp ozone (red) is also shown shifted by 5.8 ppb to
 946 match the lidar ozone (cyan), in part the black, in part the blue curve. Differences exist in the tropopause region,
 947 which is frequently the case. The sawtooth structure in the MOHp data is due to insufficient digital resolution in
 948 the NDACC data base.
 949



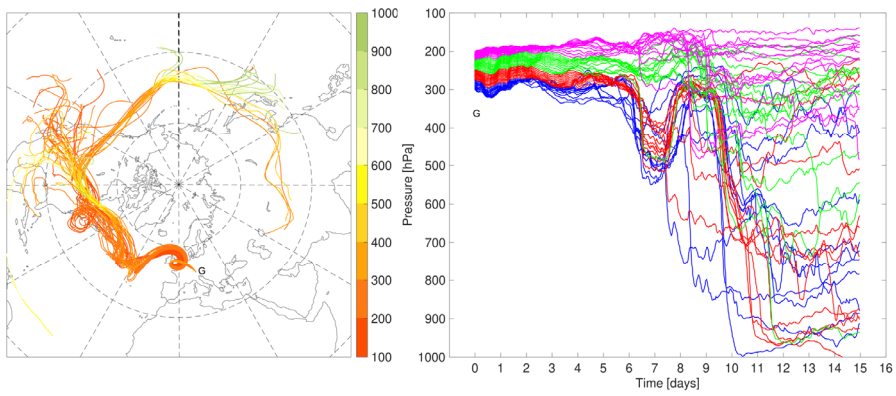
951 **Fig. 5.** Summertime ozone measurements (July 9, 2018) with pronounced layering; the sonde ozone (red) is
 952 brought to reasonable agreement with the lidar (black curve) above 2.7 km by adding 6 ppb (cyan curve). Above
 953 9 km the air masses are no longer comparable. The particularly strong discrepancy of the UFS in-situ ozone can
 954 be explained by orographic lifting of the ozone edge at 2.7 km. The moderate RH (grey) in the free troposphere
 955 indicates that the very high ozone values could be due to a stratospheric air component.
 956

Irupdwluw#kuliw@u#xuvly

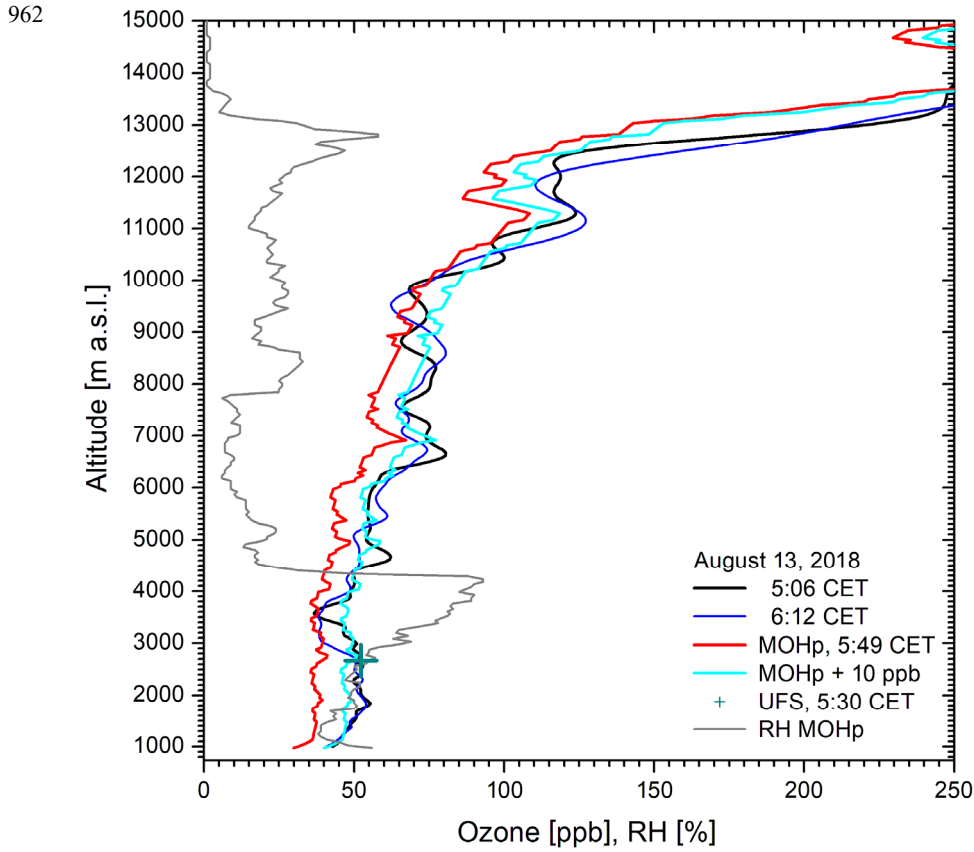
957



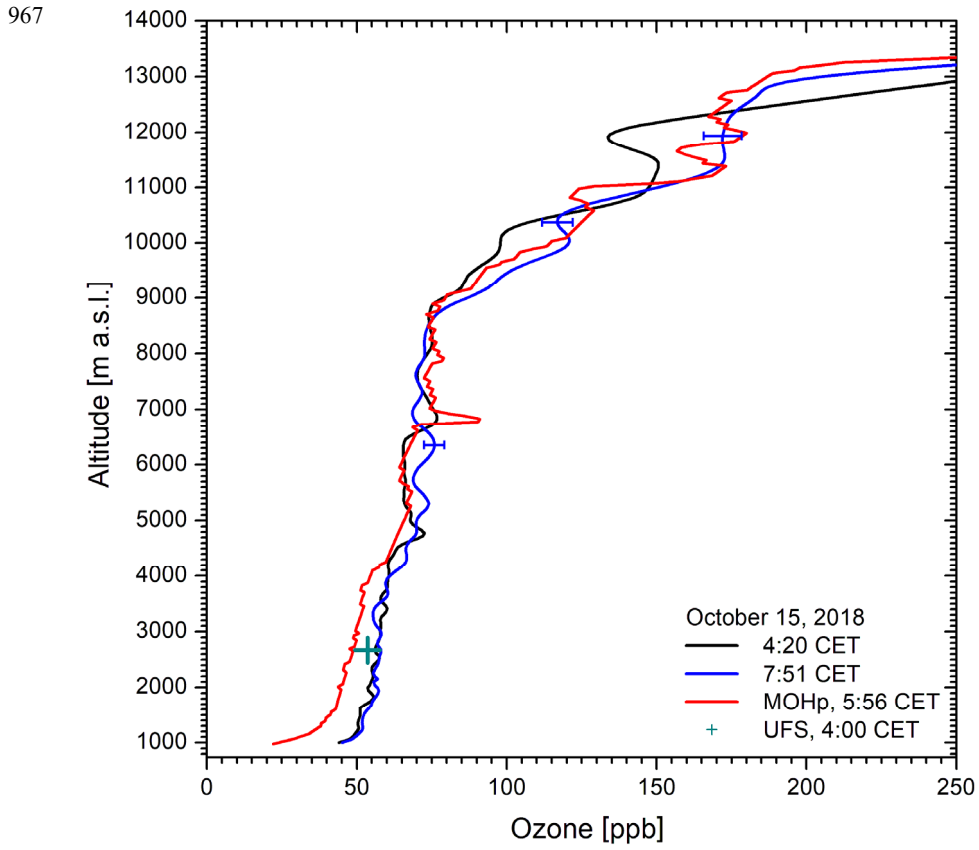
958 **Fig. 6.** 350-h LAGRANTO backward trajectories, started above Garmisch-Partenkirchen (G) on 9 July 2018 at
959 7:00 CET



960 **Fig. 7.** 350-h LAGRANTO backward trajectories, started above Garmisch-Partenkirchen (G) on 9 July 2018 at
961 8:00 CET

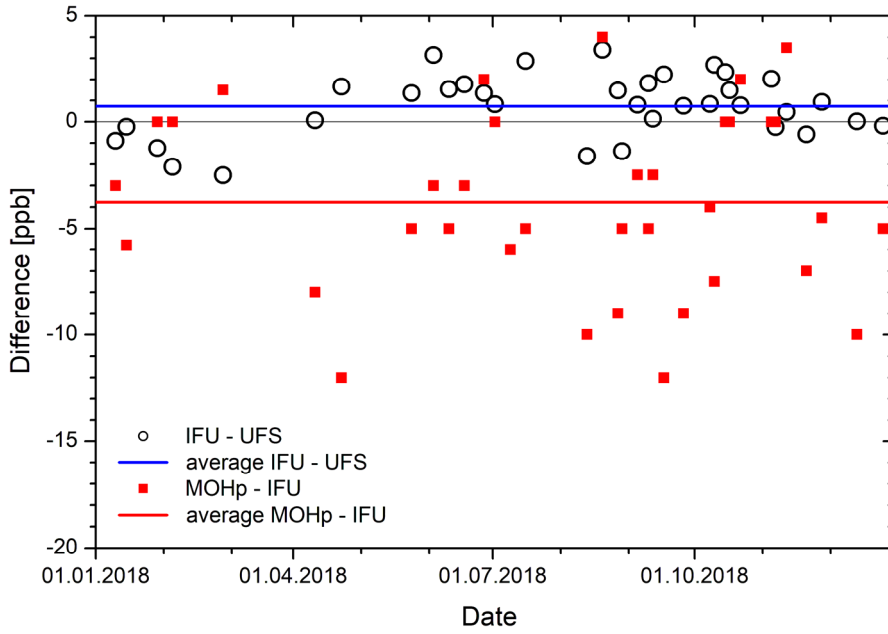


963 **Fig. 8.** Ozone measurements on 13 August 2018: The agreement of the shifted MOHp ozone profile (cyan) with
 964 the lidar curves is rather good up to 12 km given the high summertime variability. The low to moderate RH
 965 above 4.4 km (grey) indicates that the elevated ozone is partially caused by stratospheric air.
 966

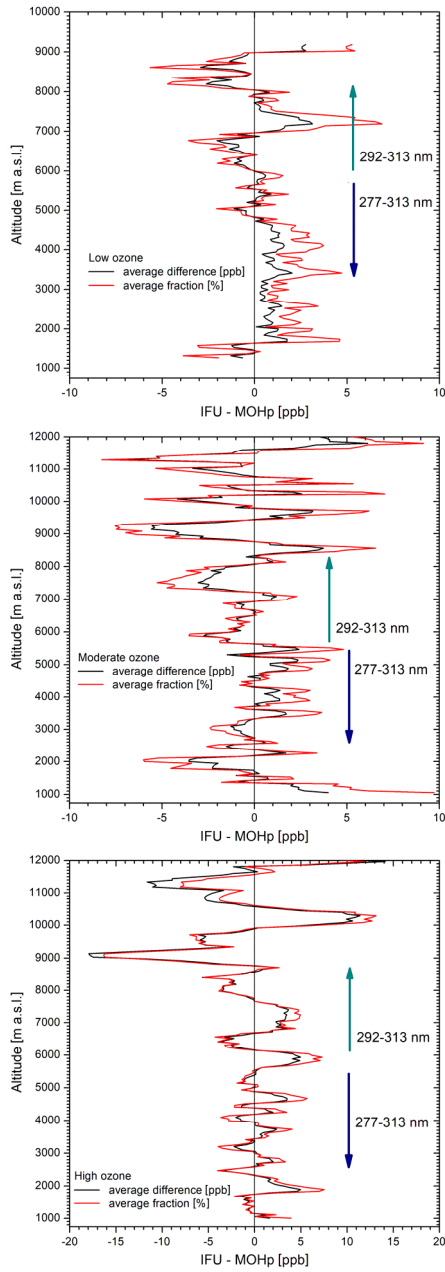


968 **Fig. 9.** Ozone measurements on 15 October 2018: The MOHp ozone (red) is not shifted. The agreement above
 969 4.3 km is better with the earlier lidar measurement (black), above 7 km better with the blue curve. The lidar data
 970 are strongly smoothed in the stratosphere, as can be seen from the more detailed ozone structure in the sonde
 971 data. This example is one of the two examples with a pronounced low-altitude discrepancy between lidar and
 972 sonde extending to more the 3 km.
 973

974

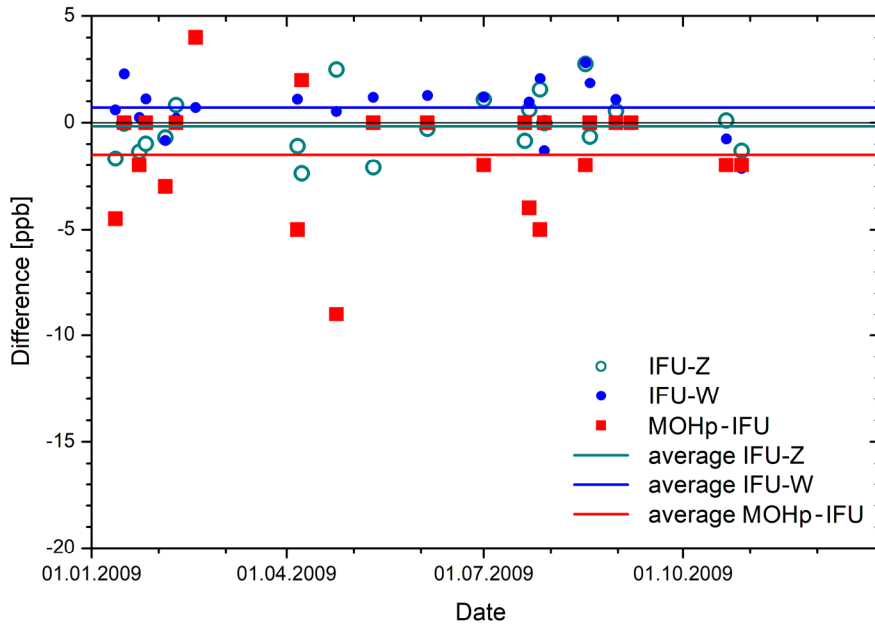


975 **Fig. 10.** Differences between the ozone values of the IFU DIAL at 2670 m and the UFS routine measurements as
976 well as the offsets of the MOHp profiles with respect to the DIAL for 35 of the 36 measurement days of the 2018
977 comparison. The blue curve represents a ± 2 -point running average of the differences between lidar and station.
978

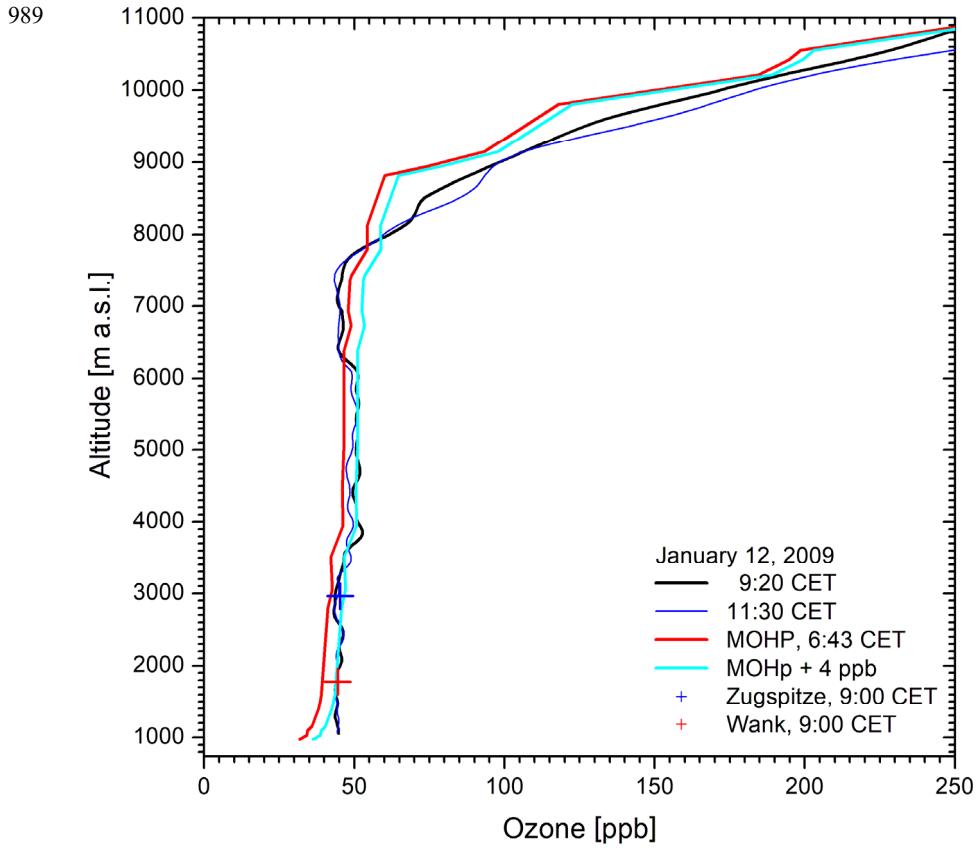


980 **Fig. 11.** Average differences between IFU lidar and offset-corrected MOHp sonde in 2018 for low-, moderate
 981 and high-conditions (based on six, seven and six comparisons, respectively); the uncertainties may be estimated
 982 from the maximum differences around the respective altitudes. We also indicate the approximate altitude ranges
 983 of the two wavelength pairs used for the lidar data evaluation.
 984

985

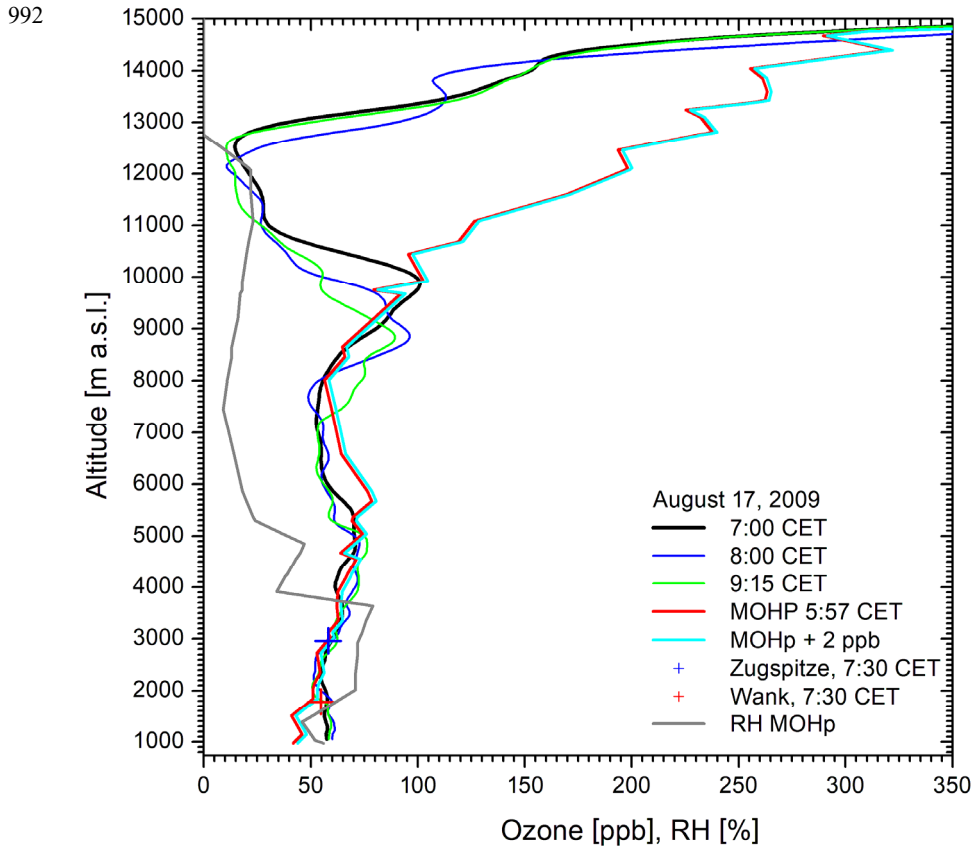


986 **Fig. 12.** Differences between the ozone mixing ratios of the lidar (IFU) and the stations Zugspitze (Z), Wank
987 (W) at the summit altitudes, and offsets between lidar and MOHp sonde for 2009
988



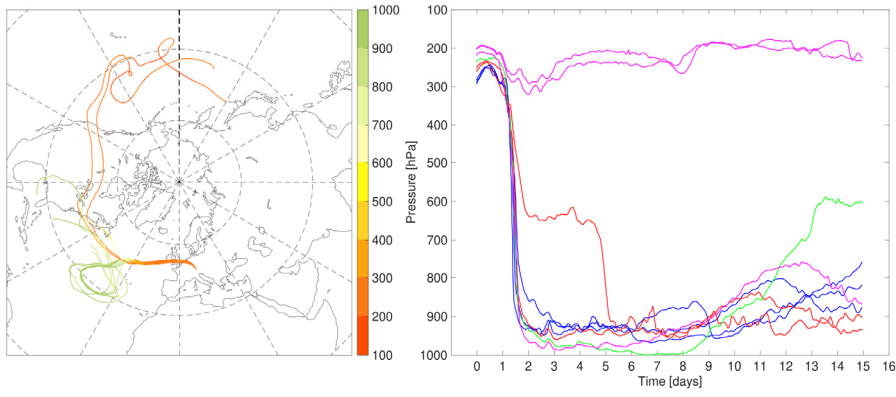
990 **Fig. 13.** Ozone measurements on 12 January 2009

991

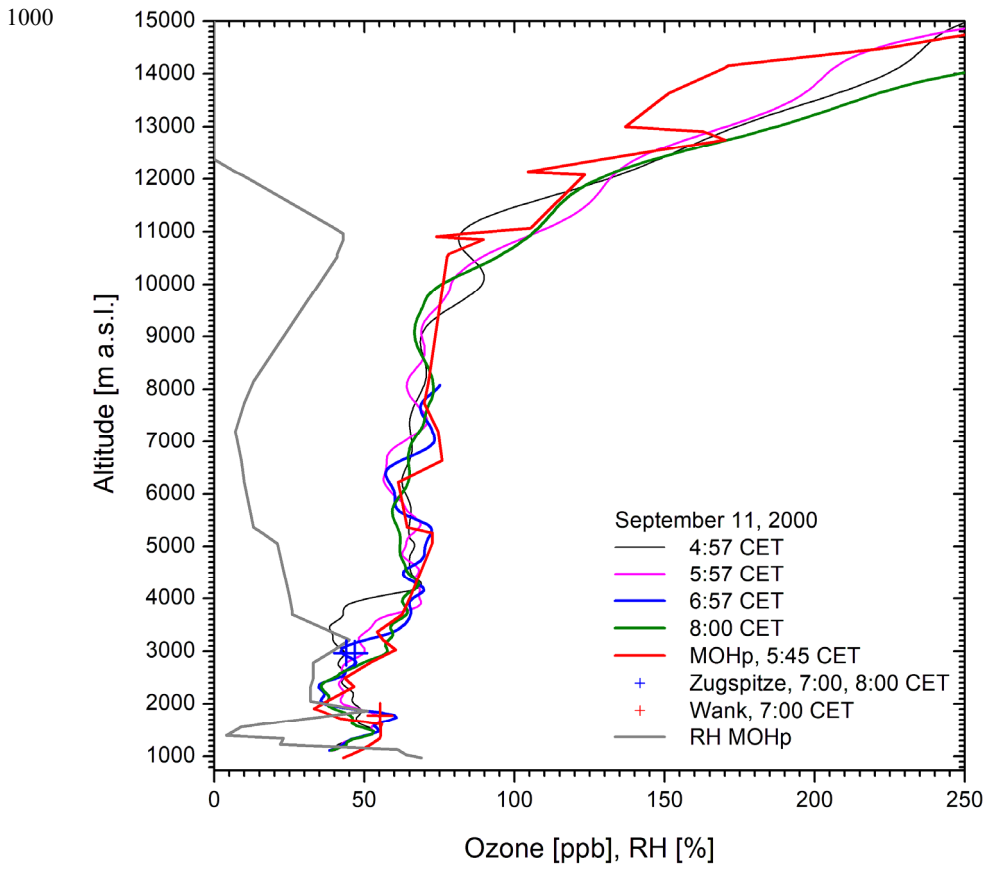


993 **Fig. 14.** Ozone measurements on 17 August 2009; the structure in the upper troposphere is strongly influenced
 994 by smoothing. The bias between 5.5 and 8 km has not been explained.
 995

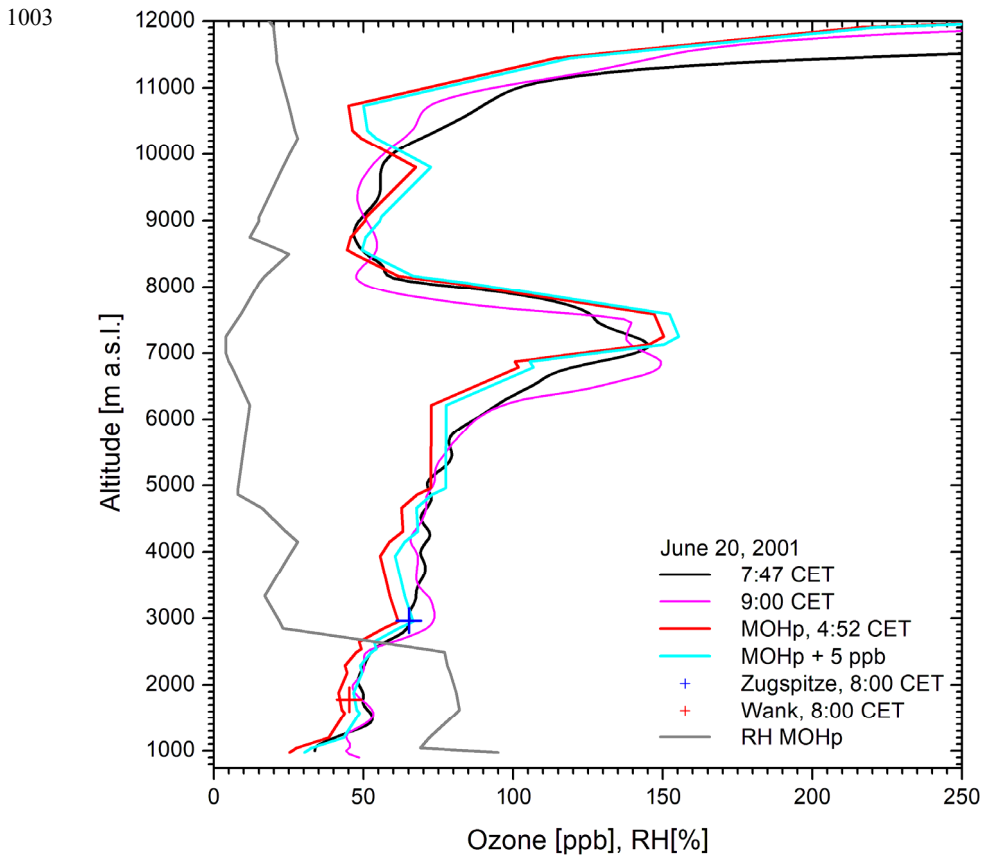
996



997 **Fig. 15.** 350-h LAGRANTO backward trajectories, started above Garmisch-Partenkirchen (G) on 9 July 2018 at
998 7:00 CET
999

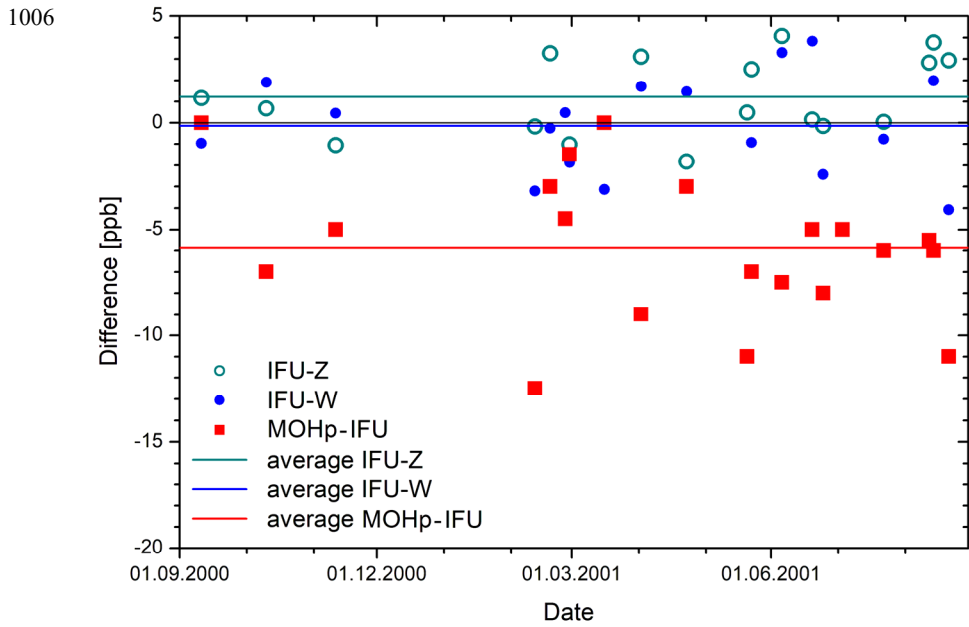


1001 Fig. 16. Ozone measurements on 11 September 2000; in this case no offset was determined.
 1002



1004 **Fig. 17.** Ozone measurements on 20 June, 2001

1005



1007 **Fig. 18.** Differences between the ozone mixing ratios of the lidar (IFU) and the stations Zugspitze (Z), Wank
 1008 (W) at the summit altitudes, and between lidar and MOHp sonde, determined by shifting the sonde profile, for
 1009 2009.

1010
 1011
 1012